J Sci Comput (2017) 72:252–290
DOI 10.1007/s10915-016-0355-x

On the Development of a Nonprimitive Navier–Stokes Formulation Subject to Rigorous Implementation of a New Vorticity Integral Condition

Shuvam Sen[1] · **Tony W. H. Sheu**[2,3,4]

Received: 21 August 2015 / Revised: 29 December 2016 / Accepted: 30 December 2016 /
Published online: 7 January 2017

Abstract In this paper, a new integral vorticity boundary condition has been developed and implemented to compute solution of nonprimitive Navier–Stokes equation. Global integral vorticity condition which is of primitive character can be considered to be of entirely different kind compared to other vorticity conditions that are used for computation in literature. The procedure realized as explicit boundary vorticity conditions imitates the original integral equation. The main purpose of this paper is to design an algorithm which is easy to implement and versatile. This algorithm based on the new vorticity integral condition captures accurate vorticity distribution on the boundary of computational flow field and can be used for both wall bounded flows as well as flows in open domain. The approach has been arrived at without utilizing any *ghost* grid point outside of the computational domain. Convergence analysis of this alternative vorticity integral condition in combination with semi-discrete centered difference approximation of linear Stokes equation has been carried out. We have also computed correct pressure field near the wall, for both attached and separated boundary layer flows, by using streamfunction and vorticity field variables. The competency of the proposed boundary methodology *vis-a-vis* other popular vorticity boundary conditions has been amply appraised by its use in a model problem that embodies the essential features of the incompressibility and viscosity. Subsequently the proposed methodology has been further validated by computing analytical solution of steady Stokes equation. Finally, it has been applied to three benchmark problems governed by the incompressible Navier–Stokes

✉ Tony W. H. Sheu
twhsheu@ntu.edu.tw

Shuvam Sen
shuvam@tezu.ernet.in

1 Department of Mathematical Sciences, Tezpur University, Tezpur 784028, India

2 Taida Institute of Mathematical Sciences, National Taiwan University, Taipei 10617, Taiwan, ROC

3 Center for Advanced Study in Theoretical Science, National Taiwan University, Taipei 10617, Taiwan, ROC

4 Department of Engineering Science and Ocean Engineering, National Taiwan University, Taipei 10617, Taiwan, ROC

equations, *viz.* lid driven cavity, backward facing step and flow past a circular cylinder. The results obtained are in excellent agreement with computational and experimental results available in literature, thereby establishing efficiency and accuracy of the proposed algorithm. We were able to accurately predict both vorticity and pressure fields.

Keywords Vorticity integral condition · Vorticity field · Pressure field · Navier–Stokes equations

Mathematics Subject Classification 65M06 · 65N06 · 76D05 · 76M20

1 Introduction

Primitive variable and streamfunction–vorticity ($\psi-\omega$) formulations of Navier–Stokes (N–S) equations are the most sought approaches for computing viscous incompressible fluid flows. Both approaches have their own advantages and disadvantages. The main advantage with the primitive variable formulation is that it directly predicts velocity and pressure fields whereas the $\psi-\omega$ formulation has the advantage that it ensures exact and automatic satisfaction of mass conservation equation. Primitive variable formulation has the traditional difficulty because of the presence of pressure term in the governing equations. A typical difficulty with the $\psi-\omega$ formulation is that in three dimensions one needs to deal with six unknowns in six equations in addition to the complexities associated with vorticity boundary conditions. For flows in two dimensions, $\psi-\omega$ formulation is more popular for its computational economy. The coupled system of the equations for vorticity and streamfunction, which are the transport equation and the Poisson equation, respectively, gives a scalar representation of the governing equations and can be used for both steady and unsteady simulations. However the typical issue arising due to the lack of a clear prescription of the ω on the boundaries persists. Further ψ is supplemented by over specification, precisely two, as far as boundary conditions are concerned. Essentially the velocity boundary condition provides two conditions on the streamfunction and its normal derivative but none on the vorticity.

Here it is worthwhile to point out that there are two other increasingly popular non-primitive approaches to tackle N–S equations. The first one is the vorticity–velocity approach. A complete review of this approach was carried out by Gatski [1]. It is noted that vorticity also needs to be tackled correctly at the boundary. Moreover in three dimensions this approach does require solution for six dependent variables. The second non-primitive approach due to Gupta and Kalita [2] is known as the streamfunction–velocity formulation. In that approach, although the problem of vorticity boundary condition is obliterated but the formulation leads to a biharmonic equation.

The subject of the vorticity boundary condition dates back to 1930s. It is well known that for a wall bounded flow correct and accurate imposition of vorticity boundary condition is extremely important as the vorticity is conserved at the interior points and transport equation determines how ω is advected and diffused. It is only the diffusion and advection of the vorticities produced at no slip boundaries that drive the flow. In literature [3–5] one can find different classes of methods that have been proposed for correct determination of the vorticity boundary values.

The first attempt to derive wall vorticity condition can be found in the pioneering work of Thom [6]. He derived a local formula whose Taylor series expansion indicates first order accurate approximation of Eq. (2) at the wall. But since then different authors [4,5,7] have

demonstrated that Thom's formula, in the context of coupled approaches, is indeed second order accurate approximation of the two boundary conditions for ψ and is consistent with a centered finite difference discretization of the streamfunction–vorticity formulation. Thom's formula ever since has been used extensively. With the advent of electronic computers there has been a surge in the derivation of more accurate local boundary conditions. Many of them have been derived by assuming enough regularity of the flow variables so that streamfunction–vorticity formulation is valid on the boundary. Note that sufficient condition to extend $\psi-\omega$ formulation from Ω to $\overline{\Omega}$, where Ω is the domain under consideration, is that ω is Lipschitz continuous, which is much less a regularity requirement compared to the assumptions involved in the process of discretization at the internal nodal points. But it was quickly perceived that the use of higher order discretization in the boundary makes the overall scheme less stable. Numerical instability was reported in some cases where vorticity boundary values were specified in terms of streamfunction without a relaxation process on the boundary. A complete review of the early development of higher order local vorticity boundary conditions and their stability characteristics can be found in the works of Roache [3] and Orszag and Israeli [8].

Other physically and mathematically rigorous means to circumvent the problem of boundary condition associated with $\psi-\omega$ formulation is to use either a biharmonic form of the N–S equation or to get into a mathematically equivalent vorticity integral condition. Although schemes have been designed for the biharmonic form [9–11], such exertions require to handle fourth order non-linear equations as compared to the second order equations for $\psi-\omega$ system. On the other hand precise mathematical condition on the vorticity, which is fundamentally more primitive in nature, for the equations of viscous incompressible flow in two and three dimensions was established by Quartapelle and Valz-Gris [12]. Important contributions on these global integral vorticity conditions and their implementation were made among others by Quartapelle et al. [5,12], Chorin [13] and Anderson [14]. In these works the principal assumption is that the boundary conditions on the velocity induce a constraint on the vorticity. Quartapelle and Valz-Gris [12] make use of this constraint and argue that the space of the discrete harmonic functions orthogonal to the discrete vorticity field contains exactly as many linearly independent functions as the number of boundary points. These linearly independent functions are then used to obtain the required number of algebraic equations needed to close the system of equations resulting from the spatial discretization of the vorticity transport equation. For implicit treatment of the vorticity diffusion term, the system of algebraic equations corresponding to the boundary points is coupled and implicit, involving vorticity and the streamfunction, and hence possess difficulty in computing solution. Anderson [14] on the other hand uses Green's function in the flow domain to derive conditions which ensure that as vorticity evolves the constraint is automatically satisfied. The resulting discrete boundary condition, which is derived by using a discretized form of the Green's function, ensures that the constraint is satisfied up to numerical roundoff at every time step. Care is also taken to ensure that the discrete time difference of the constraint vanishes and the initial vorticity field satisfies the constraint. All these stipulations ultimately lead to an implicit system connecting the boundary points and the corresponding solution strategy may be quite involved.

Nevertheless the use of global vorticity integral condition has not been admired well by the computational fluid dynamics community. This may be partly due to the nonlocal and nonlinear nature of the global vorticity integral condition. Further Weinan and Liu [4] in their work have shown that many of these global vorticity boundary conditions are actually the same as some of the local formula. In general implementation of global integral condition leads to a coupled system of equations involving vorticity and streamfunction at different boundary points and is much more intricate to implement as compared to the local ones [4].

The primary aim of this manuscript is to design a new explicit algorithm based on a newly formulated integral vorticity boundary condition. The algorithm thus designed should be able to simulate vorticity on the computational boundary under different physical and geometrical conditions. Further it should be straightforward as far as implementation is concerned.

In this paper we introduce a new rigorous integral vorticity boundary condition and hence design a family of vorticity boundary algorithms which can be used to develop efficient finite difference methods using vorticity as variable. This new algorithm, although contains interior values of the gradients of ψ, can be realized using an explicit formula. It can be applied with ease in different geometric settings and is able to tackle both wall bounded and open flow problems.

In this work we will use an implicit spatially fourth order accurate compact finite difference scheme for discretizing both vorticity and streamfunction equations. The scheme [15], developed recently for unsteady convection–diffusion equation with variable convection coefficients, is second order accurate in time. This scheme carries transport variable and its first derivatives as the unknowns and enjoys better resolution properties and hence lesser dissipation error when compared to other compact schemes. The scheme was found to be quite successful in solving N–S equations.

The rest of this paper is organized into four sections. In Sect. 2 we present the mathematical model of boundary condition and the governing equations. Section 3 deals with numerical implementation including convergence analysis. Results have been discussed in Sect. 4 and finally in Sect. 5 concluding remarks are offered.

2 Mathematical Model

The streamfunction–vorticity formulation of the N–S equations for incompressible viscous fluid flows in two dimension can be written as

$$\frac{\partial}{\partial t}\omega + J(\omega, \psi) = \frac{1}{Re}\nabla^2\omega, \tag{1}$$

$$-\nabla^2\psi = \omega, \tag{2}$$

where $J(\omega, \psi) = \dfrac{\partial(\omega, \psi)}{\partial(x, y)}$ is the Jacobian. Here ω is the out-of-plane component of vorticity vector and ψ is the streamfunction. Further $Re = \frac{UL}{\nu}$ is the Reynolds number based on the characteristic length L and the characteristic velocity U of the flow.

The boundary conditions for the above elliptic–parabolic differential system can be derived by separating the normal and tangential components of the velocity at the boundary. The boundary conditions for ψ can be written down as

$$\psi|_{\partial\Omega} = a, \quad \left.\frac{\partial\psi}{\partial \boldsymbol{n}}\right|_{\partial\Omega} = b \tag{3}$$

where Ω is the domain under consideration and $\boldsymbol{n}$ is the outward unit normal. Thus it appears that as one transforms from primitive variables to the streamfunction–vorticity form boundary conditions for the vorticity are eluded and two boundary conditions are given for the streamfunction. Note that this does not mean that the problem is over-determined rather the system with these boundary conditions is correctly posed. In fact, the system can be solved in a coupled manner where the vorticity field is required to satisfy solvability condition given as

$$\int_{\Omega} \omega dV = -\oint_{\partial\Omega} b ds. \tag{4}$$

Also the problem of lack of boundary condition for vorticity can be circumvented by using the biharmonic form which eliminates the vorticity variable altogether. However Quartapelle [5,12] has shown that the equations for the vorticity can be closed by adjoining a constraint which ensures that the boundary conditions given in Eq. (3) are simultaneously satisfied. We reproduce the following theorem found in [5,12] for completeness.

Theorem 1 *A function ω defined in the plane domain Ω is such that $\omega = -\nabla^2\psi$, with $\psi|_{\partial\Omega} = a$, and $\frac{\partial\psi}{\partial \boldsymbol{n}}\big|_{\partial\Omega} = b$, if and only if*

$$\int_{\Omega} \omega\eta dV = \oint_{\partial\Omega} \left(a\frac{\partial\eta}{\partial \boldsymbol{n}} - b\eta \right) ds \tag{5}$$

for any η harmonic in Ω, i.e. any function η such that $\nabla^2\eta = 0$ in Ω.

Authors in [5,12] considered the above integral condition to be of primitive type and concluded that this type of integral condition can be thought of as a new legitimate substitute for boundary condition required for supplementing the second order parabolic or elliptic equations beyond Dirichlet and Neumann conditions. Thus the vorticity integral condition Eq. (5) can be used to serve as a boundary condition for vorticity transport equation (1), whereas $\psi|_{\partial\Omega} = a$ can continue to act as the Dirichlet boundary condition for elliptic streamfunction equation (2).

The main convolution involved with the application of vorticity integral condition is the obligation to store as many discrete harmonic functions as the number of boundary points in the discrete space. These harmonic functions will then lead to a full system of equations whose order equates the number of boundary points. Finally, at each time step, inversion of this system provides correct vorticity boundary values. This implicit computation is by and large quite expensive. To overcome this intricacy we modify Theorem 1 to propose a new vorticity boundary condition.

Theorem 2 *A function ω defined in the plane domain Ω is such that $\omega = -\nabla^2\psi$, with $\psi|_{\partial\Omega} = a$, and $\frac{\partial\psi}{\partial \boldsymbol{n}}\big|_{\partial\Omega} = b$, if and only if*

$$\int_{\Omega_j} \omega dV = -\oint_{\partial\Omega_j \cap \partial\Omega} b ds - \oint_{\partial\Omega_j - \partial\Omega_j \cap \partial\Omega} \frac{\partial\psi}{\partial \boldsymbol{n}} ds \tag{6}$$

for any $\Omega_j \subseteq \Omega$ where $j \in \mathfrak{J}$, $\mathfrak{J}$ being some index set.

Proof Necessary Part: Let $\omega = -\nabla^2\psi$ be a function defined over the domain Ω with $\psi|_{\partial\Omega} = a$, and $\frac{\partial\psi}{\partial \boldsymbol{n}}\big|_{\partial\Omega} = b$. Let $\Omega_j \subseteq \Omega$ where $j \in \mathfrak{J}$, $\mathfrak{J}$ being some index set. Using the divergence theorem we get

$$\begin{aligned}
\int_{\Omega_j} \omega dV &= \int_{\Omega_j} (-\nabla^2\psi) dV \\
&= \oint_{\partial\Omega_j} -\frac{\partial\psi}{\partial \boldsymbol{n}} ds \\
&= -\oint_{\partial\Omega_j \cap \partial\Omega} \frac{\partial\psi}{\partial \boldsymbol{n}} ds - \oint_{\partial\Omega_j - \partial\Omega_j \cap \partial\Omega} \frac{\partial\psi}{\partial \boldsymbol{n}} ds \\
&= -\oint_{\partial\Omega_j \cap \partial\Omega} b ds - \oint_{\partial\Omega_j - \partial\Omega_j \cap \partial\Omega} \frac{\partial\psi}{\partial \boldsymbol{n}} ds.
\end{aligned}$$

Sufficient Part: Let ω satisfy the condition

$$\int_{\Omega_j} \omega dV = -\oint_{\partial\Omega_j \cap \partial\Omega} b ds - \oint_{\partial\Omega_j - \partial\Omega_j \cap \partial\Omega} \frac{\partial \psi}{\partial \boldsymbol{n}} ds$$

for any $\Omega_j \subseteq \Omega$ where $j \in \mathfrak{J}$, $\mathfrak{J}$ being an index set. Consider ψ to be the unique solution of the equation $-\nabla^2 \psi = \omega$ subject to the condition $\psi|_{\partial\Omega} = a$. Now we have

$$\begin{aligned}\int_{\Omega_j} \omega dV &= \int_{\Omega_j} (-\nabla^2 \psi) dV \\ &= \oint_{\partial\Omega_j} -\frac{\partial \psi}{\partial \boldsymbol{n}} ds \\ &= -\oint_{\partial\Omega_j \cap \partial\Omega} \frac{\partial \psi}{\partial \boldsymbol{n}} ds - \oint_{\partial\Omega_j - \partial\Omega_j \cap \partial\Omega} \frac{\partial \psi}{\partial \boldsymbol{n}} ds.\end{aligned}$$

Thus we see that

$$\begin{aligned}-\oint_{\partial\Omega_j \cap \partial\Omega} b ds &= -\oint_{\partial\Omega_j \cap \partial\Omega} \frac{\partial \psi}{\partial \boldsymbol{n}} ds \\ \Rightarrow \oint_{\partial\Omega_j \cap \partial\Omega} \left(b - \frac{\partial \psi}{\partial \boldsymbol{n}} \right) ds &= 0.\end{aligned}$$

Finally using the arbitrariness of Ω_j we see that $\frac{\partial \psi}{\partial \boldsymbol{n}}\big|_{\partial\Omega} = b$. □

This new vorticity integral condition Eq. (6), although global in nature, can be realized locally and provides a technique to compute vorticity boundary values explicitly. Hence it is more suitable for simulating complex flow fields. We will examine this global boundary condition in different geometric setups involving varied physical situations. The following section details its implementation.

Here we would like to point out that it may be quite possible to extend this new approach to three dimensional problems and will be explored in future. Three dimensional form of the streamfunction–vorticity formulation [16] also endures issues regarding vorticity boundary condition. Quartapelle and Valz-Gris [12] in their work have successfully generalized the vorticity integral condition given in the Eq. (5).

3 Numerical Implementation

We present here details of implementing the new vorticity integral condition Eq. (6) in finite difference setup. To begin with we note that the new condition is a perspective which can be implemented in varied fashions. The blueprint developed here is in conjunction with ideas borrowed from the staggered grid approach in finite volume and is explained in rectangular grid by developing four different schemes corresponding to the four different sub-figures of the Fig. 1. We begin by considering an elementary rectangular area, marked by black faces, in the vicinity of the left boundary. The center of the cell, marked using "•", is deemed at the mid point of the rectangular area. In this work we delve with four positions of "•" *viz.* at distances $\frac{h}{2}$, $\frac{h}{3}$, $\frac{h}{4}$ and $\frac{h}{16}$ from the boundary as shown in Fig. 1a–d, respectively. The vorticity value at this center is approximated by taking the weighted mean of the vorticity values at the boundary and the interior nodes. This mean value is used to approximate the left hand side of the integral Eq. (6). Estimation of the two integrals on the right hand side of

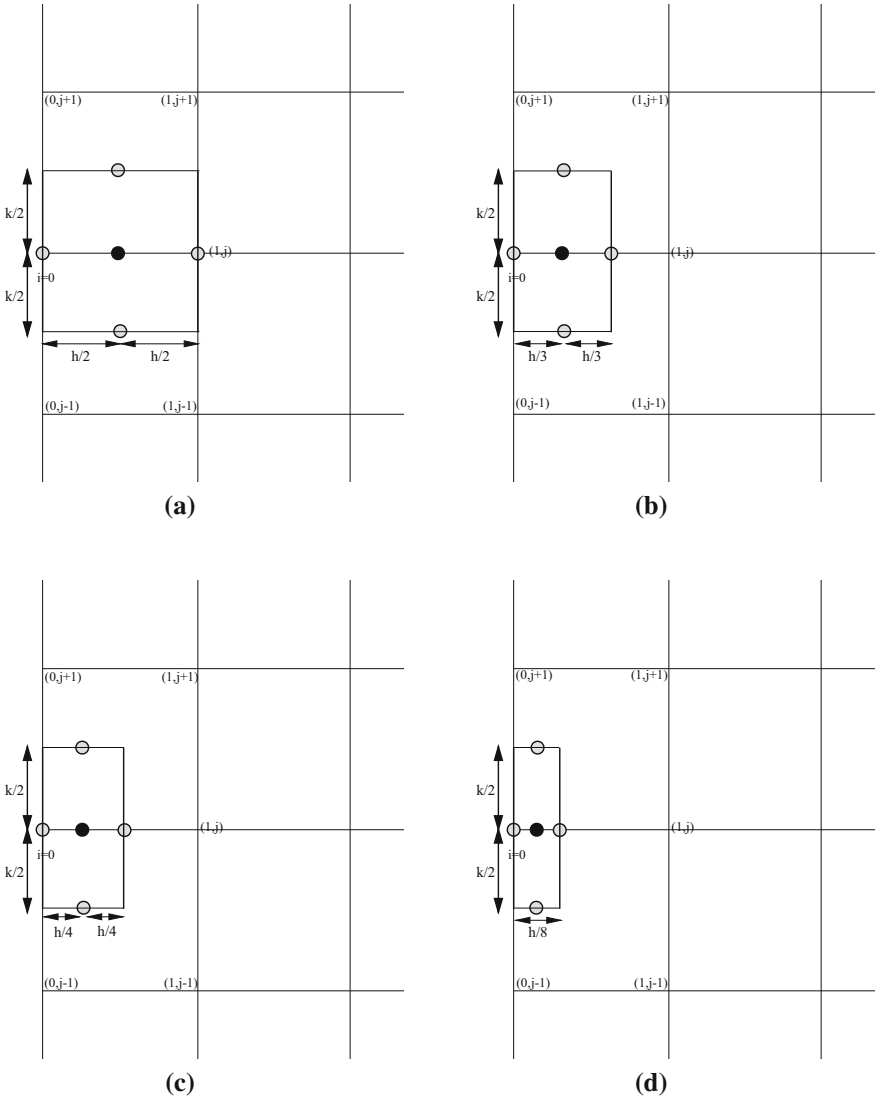

Fig. 1 Schematic diagram of four different implementations of vorticity integral condition. Depicted are the nodes used to compute vorticity at the left boundary. "•" denotes the center of the rectangular cell used to approximate the boundary condition and "∘" denotes face center at which some of the gradients of stream-function were estimated. **a** New 1 Eq. (8), **b** New 2 Eq. (9), **c** New 3 Eq. (10), **d** New 4 Eq. (11)

Eq. (6) requires knowledge of derivatives of ψ at the nodes marked using "∘"; which are in general not available. Hence these values are required to be approximated or interpolated by using ψ or its corresponding derivatives available at the vertices. We present below various techniques for estimating the integrals. The reason for choosing different cell centers is to provide an idea of how different explicit vorticity boundary conditions can be formulated based on the integral equation (6). Further we use increasingly narrow cells as such a choice will test the stability and effectiveness of Eq. (6) from the point of its implementation.

For the Fig. 1a the integrals are calculated in the simplest possible way. Here ψ_y at the top and bottom "$\circ$" nodes are interpolated by using ψ_y values at the vertices of the rectangle inside which they sit. For the uniform rectangular grid the vorticity boundary value at $(0, j)$ can thus be approximated as

$$\frac{hk}{2}(\omega_{0,j}+\omega_{1,j}) = \psi_{x_{0,j}}k - \psi_{x_{1,j}}k + \frac{h}{4}(\psi_{y_{0,j}}+\psi_{y_{1,j}}+\psi_{y_{0,j-1}}+\psi_{y_{1,j-1}}) - \frac{h}{4}(\psi_{y_{0,j}}+\psi_{y_{1,j}}+\psi_{y_{0,j+1}}+\psi_{y_{1,j+1}}).$$

Note that the above equation has been arrived at by approximating integrals of the Eq. (6). On simplification we obtain

$$\omega_{0,j} = -\omega_{1,j} + \frac{2}{h}(\psi_{x_{0,j}} - \psi_{x_{1,j}}) + \frac{1}{k^2}(-\psi_{0,j-1} + 2\psi_{0,j} - \psi_{0,j+1} - \psi_{1,j-1} + 2\psi_{1,j} - \psi_{1,j+1}) \tag{7}$$

for all $0 < j < jmax$. The truncation error corresponding to the Taylor series expansion for the Eq. (7) is

$$\frac{h^2}{6}\psi_{xxxx_{\frac{1}{2},j}} - \frac{k^2}{6}\psi_{yyyy_{\frac{1}{2},j}} + O(h^4, k^4, h^2k^2).$$

Equation (7) can also be replaced by another equivalent form

$$\omega_{0,j} = -\omega_{1,j} + \frac{2}{h}(\psi_{x_{0,j}} - \psi_{x_{1,j}}) + \frac{1}{2k}(\psi_{y_{0,j-1}} + \psi_{y_{1,j-1}} - \psi_{y_{0,j+1}} - \psi_{y_{1,j+1}}) \tag{8}$$

for all $0 < j < jmax$ with corresponding truncation error

$$\frac{h^2}{6}\psi_{xxxx_{\frac{1}{2},j}} - \frac{k^2}{3}\psi_{yyyy_{\frac{1}{2},j}} + O(h^4, k^4, h^2k^2).$$

This newly proposed formula will be refereed to as *New 1* boundary condition in the manuscript. If we restrict ourselves to second order central difference approximations to estimate $\omega_{i,j}$ and $\psi_{x_{i,j}}$ at interior nodes *i.e.* $\omega_{i,j} = -(\psi_{i-1,j} - 2\psi_{i,j} + \psi_{i+1,j})/h^2 - (\psi_{i,j-1} - 2\psi_{i,j} + \psi_{i,j+1})/k^2$ and $\psi_{x_{i,j}} = (\psi_{i+1,j} - \psi_{i-1,j})/2h$ together with homogeneous boundary conditions $\psi_{0,j} = 0$, $\psi_{x_{0,j}} = 0$ then the Eq. (7) can be reduced to

$$\omega_{0,j} = -\frac{2}{h^2}\psi_{1,j}.$$

The above simplified form of the vorticity boundary condition, which is valid under a set of assumptions, will be used for convergence analysis to be carried out in Sect. 3.1.

Another choice for estimating the gradients ψ_x and ψ_y, which correspond directly to the velocity components in the rectangular cartesian grid, is to use the fourth order Padé approximations which will be detailed once we complete different implementations of the Eq. (6). Here it is worthwhile to point out that varied approximations of stream function gradients can be used in conjunction with Eq. (8).

Boundary conditions on the right, bottom and top boundaries can be found likewise and are written below for totality.

$$\omega_{imax,j} = -\omega_{imax-1,j} + \frac{2}{h}(\psi_{x_{imax-1,j}} - \psi_{x_{imax,j}}) + \frac{1}{2k}(\psi_{y_{imax,j-1}} + \psi_{y_{imax-1,j-1}} - \psi_{y_{imax,j+1}} - \psi_{y_{imax-1,j+1}})$$

for all $0 < j < jmax$.

$$\omega_{i,0} = -\omega_{i,1} + \frac{2}{k}(\psi_{y_{i,0}} - \psi_{y_{i,1}}) + \frac{1}{2h}(\psi_{x_{i-1,0}} + \psi_{x_{i-1,1}} - \psi_{x_{i+1,0}} - \psi_{x_{i+1,1}})$$

for all $0 < i < imax$.

$$\omega_{i,jmax} = -\omega_{i,jmax-1} + \frac{2}{k}(\psi_{y_{i,jmax-1}} - \psi_{y_{i,jmax}}) + \frac{1}{2h}(\psi_{x_{i-1,jmax}} + \psi_{x_{i-1,jmax-1}} - \psi_{x_{i+1,jmax}} - \psi_{x_{i+1,jmax-1}})$$

for all $0 < i < imax$.

Again for the Fig. 1b the vorticity value at the cell center, located at $\left(\frac{h}{3}, j\right)$, is approximated as

$$\omega_{1/3,j} = \frac{1}{3}(2\omega_{0,j} + \omega_{1,j}).$$

Also ψ_y value at the top "$\circ$" node is interpolated as

$$\psi_{y_{1/3,j+1/2}} = \frac{1}{3}(2\psi_{y_{0,j+1/2}} + \psi_{y_{1,j+1/2}})$$

where $\psi_{y_{i,j+1/2}} = \frac{\psi_{i,j+1} - \psi_{i,j}}{k}$, $i = 0, 1$. Similar expression also holds for lower "$\circ$" node. Finally the $\psi_{x_{2/3,j}}$ value at the middle "$\circ$" node is linearly interpolated by using $\psi_{x_{1/2,j}} = \frac{\psi_{1,j} - \psi_{0,j}}{h}$ and $\psi_{x_{1,j}}$. Thus the approximation of integral condition Eq. (6) yields for the left boundary

$$\begin{aligned}
\omega_{1/3,j}\frac{2h}{3}k &= \psi_{x_{0,j}}k - \psi_{x_{2/3,j}}k + \psi_{y_{1/3,j-1/2}}\frac{2h}{3} - \psi_{y_{1/3,j+1/2}}\frac{2h}{3} \\
\Rightarrow \omega_{0,j} &= -\frac{1}{2}\omega_{1,j} + \frac{3}{2}\Bigg[\frac{3}{2h}\left(\psi_{x_{0,j}} - \left(\frac{2}{3}\frac{\psi_{1,j} - \psi_{0,j}}{h} + \frac{1}{3}\psi_{x_{1,j}}\right)\right) \\
&\quad + \frac{1}{3k^2}\left(-2\psi_{0,j-1} + 4\psi_{0,j} - 2\psi_{0,j+1} - \psi_{1,j-1} + 2\psi_{1,j} - \psi_{1,j+1}\right)\Bigg]
\end{aligned} \tag{9}$$

for all $0 < j < jmax$. The truncation error for the Eq. (9) is

$$-\frac{h}{8}\psi_{xxx_{\frac{1}{3},j}} - \frac{k^2}{8}\psi_{yyyy_{\frac{1}{3},j}} + O(h^2, k^4, h^2k^2)$$

and we referrer it as *New 2*.

Similarly for the Fig. 1c, for the cell center located at $\left(\frac{h}{4}, j\right)$ the vorticity boundary condition on the left boundary may be expressed as

$$\begin{aligned}
\omega_{0,j} &= -\frac{1}{3}\omega_{1,j} + \frac{4}{3}\Bigg[\frac{2}{h}\left(\psi_{x_{0,j}} - \frac{\psi_{1,j} - \psi_{0,j}}{h}\right) \\
&\quad + \frac{1}{4k^2}\left(-3\psi_{0,j-1} + 6\psi_{0,j} - 3\psi_{0,j+1} - \psi_{1,j-1} + 2\psi_{1,j} - \psi_{1,j+1}\right)\Bigg]
\end{aligned} \tag{10}$$

for all $0 < j < jmax$. It will be referred as *New 3* and its truncation error is

$$-\frac{h}{9}\psi_{xxx_{\frac{1}{4},j}} - \frac{k^2}{9}\psi_{yyyy_{\frac{1}{4},j}} + O(h^2, k^4, h^2k^2).$$

Finally to evaluate the effectiveness of the vorticity integral condition expressed in Eq. (6) we consider a very small cell with its center located at $\left(\frac{h}{16}, j\right)$ in the Fig. 1d. For this case the vorticity boundary condition on the left boundary has been obtained as

$$\omega_{0,j} = -\frac{1}{15}\omega_{1,j} + \frac{16}{15}\left[\frac{8}{h}\left(\psi_{x_{0,j}} - \left(\frac{21}{32}\psi_{x_{0,j}} + \frac{14}{32}\frac{\psi_{1,j}-\psi_{0,j}}{h} - \frac{3}{32}\psi_{x_{1,j}}\right)\right) + \frac{1}{16k^2}\left(-15\psi_{0,j-1} + 30\psi_{0,j} - 15\psi_{0,j+1} - \psi_{1,j-1} + 2\psi_{1,j} - \psi_{1,j+1}\right)\right] \tag{11}$$

for all $0 < j < jmax$, with truncation error given by

$$-\frac{7h}{45}\psi_{xxx_{\frac{1}{16},j}} - \frac{4k^2}{45}\psi_{yyyy_{\frac{1}{16},j}} + O(h^2, k^4, h^2k^2).$$

Note that in the above formula, termed as *New 4*, the ψ_x value at the middle "$\circ$" point shown in Fig. 1d has been quadratically interpolated.

All the above approximations of the vorticity boundary conditions *viz.* Eqs. (8)–(11) are explicit. Also since the off-grid unknown values of gradients of ψ and ω involved in all the formulas are evaluated using a linear reconstruction, they may provide the identical accuracy. But here it should be pointed out that it will be naive to conclude about the accuracy without going into a detailed analysis as has been demonstrated by Huang and Wetton [7] for Thom's formula. Such an effort for these newly developed boundary formulae will indeed be taken up in future. Presently based on Taylor expansion we can say that Eq. (8) possesses second order truncation error and the rest first order. In the later part of this section we shall highlight a few more second order accurate implementations of the integral boundary condition expressed in Eq. (6).

We intend to discretize the governing equations (1) and (2) using a recently developed compact spatially fourth and temporally second order accurate scheme [15]. This scheme which carries gradients of the transport variable as unknowns, also uses the Padé approximations

$$\psi_{x_{i,j}} = \left(\delta_x\psi_{i,j} - \frac{h^2}{6}\delta_x^2\psi_{x_{i,j}}\right) + O(h^4) \tag{12}$$

and

$$\psi_{y_{i,j}} = \left(\delta_y\psi_{i,j} - \frac{k^2}{6}\delta_y^2\psi_{y_{i,j}}\right) + O(k^4). \tag{13}$$

and hence will be computationally much more efficient in implementing the new vorticity integral condition. The finite difference approximations of Eqs. (1) and (2), valid at all internal grid points, can thus be written as

$$\left[Re - \delta t\left(\delta_x^2 + \delta_y^2\right)\right]\omega_{i,j}^{(n+1)} = \left[Re + \delta t\left(\delta_x^2 + \delta_y^2\right)\right]\omega_{i,j}^{(n)} + \frac{\delta t}{2}\left[-\left(\delta_x + Re\psi_{y_{i,j}}^{(n+1)}\right)\omega_{x_{i,j}}^{(n+1)} - \left(\delta_y - Re\psi_{x_{i,j}}^{(n+1)}\right)\omega_{y_{i,j}}^{(n+1)}\right] + \frac{\delta t}{2}\left[-\left(\delta_x + Re\psi_{y_{i,j}}^{(n)}\right)\omega_{x_{i,j}}^{(n)} - \left(\delta_y - Re\psi_{x_{i,j}}^{(n)}\right)\omega_{y_{i,j}}^{(n)}\right] \tag{14}$$

and

$$-2\delta_x^2\psi_{i,j} - 2\delta_y^2\psi_{i,j} + \delta_x\psi_{x_{i,j}} + \delta_y\psi_{y_{i,j}} = \omega_{i,j} \tag{15}$$

respectively. The solution strategy for solving Eqs. (14) and (15) consists of two steps: (a) one outer temporal loop and (b) an inner loop where we employ correcting to convergence strategy. The system of algebraic equations has been solved by using bi-conjugate gradient stabilized (BiCGStab) method [17]. The algorithm to time march the solution from (n)th to $(n+1)$th level can be found in [15] and is reproduced below for readers' convenience.

Algorithm to Time March Solution

We begin by introducing the notations: $\Psi = (\psi_{1,1}, \psi_{1,2}, ..., \psi_{m,n})^T$, $\Upsilon = (\omega_{1,1}, \omega_{1,2}, ..., \omega_{m,n})^T$ for a grid of size $m \times n$. The resulting system of equations corresponding to Eqs. (12), (13), (14) and (15) in matrix form can be written as

$$M_1 \Psi_x^{(n)} = F_1\big(\Psi^{(n)}\big), \tag{16}$$

$$M_2 \Psi_y^{(n)} = F_2\big(\Psi^{(n)}\big), \tag{17}$$

$$M_3 \Upsilon^{(n+1)} = F_3\big(\Upsilon^{(n)}, \Upsilon_x^{(n)}, \Upsilon_y^{(n)}, \Psi_x^{(n)}, \Psi_y^{(n)}, \Upsilon_x^{(n+1)}, \Upsilon_y^{(n+1)}, \Psi_x^{(n+1)}, \Psi_y^{(n+1)}\big), \tag{18}$$

$$M_4 \Psi^{(n+1)} = F_3\big(\Upsilon^{(n+1)}, \Psi_x^{(n+1)}, \Psi_y^{(n+1)}\big). \tag{19}$$

Here M_1, M_2, M_3 and M_4 are banded diagonally dominant matrices of dimension mn. The entire strategy can be summarized in the following algorithm:

1. Begin with $\Psi^{(n)}$, $\Upsilon^{(n)}$.
2. Obtain $\Psi_x^{(n)}$ and $\Psi_y^{(n)}$ using (16) and (17) respectively.
3. Similarly obtain $\Upsilon_x^{(n)}$ and $\Upsilon_y^{(n)}$.
4. Take $\Psi_{old}^{(n+1)} = \Psi^{(n)}$, $\Psi_{x_{old}}^{(n+1)} = \Psi_x^{(n)}$, $\Psi_{y_{old}}^{(n+1)} = \Psi_y^{(n)}$, $\Upsilon_{old}^{(n+1)} = \Upsilon^{(n)}$, $\Upsilon_{x_{old}}^{(n+1)} = \Upsilon_x^{(n)}$, $\Upsilon_{y_{old}}^{(n+1)} = \Upsilon_y^{(n)}$.
5. Correct to $\Upsilon_{new}^{(n+1)}$ using (18).
6. Correct to $\Upsilon_{x_{new}}^{(n+1)}$, $\Upsilon_{y_{new}}^{(n+1)}$ using (16), (17) respectively.
7. Correct to $\Psi_{new}^{(n+1)}$ using (19).
8. Correct to $\Psi_{x_{new}}^{(n+1)}$, $\Psi_{y_{new}}^{(n+1)}$ using (16), (17) respectively.
9. If $\|\Psi_{new}^{(n+1)} - \Psi_{old}^{(n+1)}\| < \epsilon$ then $\Psi^{(n+1)} = \Psi_{new}^{(n+1)}$, $\Upsilon^{(n+1)} = \Upsilon_{new}^{(n+1)}$.
10. $\Psi_{old}^{(n+1)} = \Psi_{new}^{(n+1)}$, $\Psi_{x_{old}}^{(n+1)} = \Psi_{x_{new}}^{(n+1)}$, $\Psi_{y_{old}}^{(n+1)} = \Psi_{y_{new}}^{(n+1)}$, $\Upsilon_{old}^{(n+1)} = \Upsilon_{new}^{(n+1)}$, $\Upsilon_{x_{old}}^{(n+1)} = \Upsilon_{x_{new}}^{(n+1)}$, $\Upsilon_{y_{old}}^{(n+1)} = \Upsilon_{y_{new}}^{(n+1)}$ goto step 5.

Apart from the above fourth order accurate discretizations we will also use, at a few cases, the standard second order accurate central approximation of the governing equations (1) and (2). Note that we use second or higher order accurate discretizations at the internal nodal points to restrict errors, arising out of discretization of internal nodal points, from polluting the boundary approximation.

In this study we are also interested to determine consequences of the new vorticity integral condition on the post processed pressure field especially near the boundaries. Abdallah [18] in 1987 derived second order accurate finite difference approximation for the pressure Poisson equation with Neumann boundary conditions. These approximations satisfy the mathematically necessary compatibility condition and were used in conjunction with the $\psi-\omega$ formulation to compute the pressure field. We will use the formulation of Abdallah to conclude about the effect of the new integral vorticity boundary condition on the pressure field.

3.1 Convergence Analysis

In this section we carry out convergence analysis of the newly developed boundary conditions applied to the linear system of Stokes equations:

$$\frac{\partial \omega}{\partial t} = \frac{1}{Re}\nabla^2 \omega, \quad -\nabla^2 \psi = \omega. \tag{20}$$

The nonlinear terms have been neglected for simplicity. The convergence analysis is carried out following the works of Wang and Liu [19] and Wang [20] and pursues the standard procedure of consistency, stability and error analysis. We consider a square computational domain $\Omega = [0, 1]^2$ with $h = k = 1/N$ together with Dirichlet boundary condition $\psi = 0$ on $\partial\Omega$. The grid points can then be denoted as $\{x_i = ih, y_j = jh,\ i, j = 0, 1, ..., N\}$. Further no-slip boundary condition $\frac{\partial \psi}{\partial \boldsymbol{n}} = 0$ is imposed on all boundaries. The semi-discrete centered difference approximation of Eq. (20) valid at the interior grid points together with boundary conditions is

$$\frac{\partial \omega}{\partial t} = \frac{1}{Re}\nabla_h^2 \omega, \quad -\nabla_h^2 \psi = \omega, \quad \psi|_{\partial\Omega} = 0, \quad \left.\frac{\partial \psi}{\partial \boldsymbol{n}}\right|_{\partial\Omega} = 0, \tag{21}$$

where

$$\begin{aligned} &\nabla_h^2 = D_x^2 + D_y^2, \\ &D_x^2 \psi_{i,j} = \frac{\psi_{i-1,j} - 2\psi_{i,j} + \psi_{i+1,j}}{h^2}, \ D_y^2 \psi_{i,j} = \frac{\psi_{i,j-1} - 2\psi_{i,j} + \psi_{i,j+1}}{h^2}. \end{aligned} \tag{22}$$

Using the above boundary values the newly developed vorticity boundary conditions Eqs. (8)–(11) are rewritten as

$$\omega_{0,j} = \frac{1}{h^2}(A_1 \psi_{1,j} + A_2 \psi_{2,j}) \tag{23}$$

where (A_1, A_2) are $(-2, 0)$, $(-5/2, 1/8)$, $(-10/3, 1/3)$ and $(-58/15, 7/15)$ for Eqs. (8), (9), (10) and (11), respectively. Clearly $-4 < A_1 \leq -2$ and $0 \leq A_2 < 1/2$. An equivalent form of the above relation which facilitates further analysis [19,20] is

$$\omega_{0,j} = \frac{1}{h^2}(B_1 \psi_{1,j} + B_2 h^2 D_x^2 \psi_{1,j}) \tag{24}$$

with $B_1 = A_1 + 2A_2$ and $B_2 = A_2$. Further subsequent to the works of Wang and Liu [19] and Wang [20] we introduce the following notations.

Definition 1 The discrete L^2-norm and L^2-inner product are defined as

$$\| \psi \| = \langle \psi, \psi \rangle^{1/2}, \quad \langle \psi, \phi \rangle = \sum_{1 \leq i,j \leq N-1} \psi_{i,j} \phi_{i,j} h^2. \tag{25}$$

For $\psi|_{\partial\Omega} = 0$, the notation $\| \nabla_h \psi \|$ denotes

$$\| \nabla_h \psi \|^2 = \sum_{j=1}^{N-1} \sum_{i=0}^{N-1} (D_x^+ \psi_{i,j})^2 h^2 + \sum_{i=1}^{N-1} \sum_{j=0}^{N-1} (D_y^+ \psi_{i,j})^2 h^2 \tag{26}$$

where

$$D_x^+ \psi_{i,j} = \frac{\psi_{i+1,j} - \psi_{i,j}}{h}, \quad D_y^+ \psi_{i,j} = \frac{\psi_{i,j+1} - \psi_{i,j}}{h}. \tag{27}$$

3.1.1 Consistency Analysis

Let ψ_e be the exact solution of the Stokes equation (20) extended smoothly to the domain $[-\delta, 1+\delta]^2$ and $\overline{\psi}_{i,j} = \psi_e(x_i, y_j)$ for $-1 \le i, j \le N+1$. Considering $\overline{\omega}_{i,j} = \nabla_h^2 \overline{\psi}_{i,j}$ for $0 \le i, j \le N$, Taylor series expansion reveals for all grid points (x_i, y_j), $0 \le i, j \le N$

$$\overline{\omega} = \omega_e + \frac{h^2}{12}(\partial_x^4 + \partial_y^4)\psi_e + O(h^4) \parallel \psi_e \parallel_{C^6} . \tag{28}$$

From Eq. (28) we see that for internal grid points (x_i, y_j), $1 \le i, j \le N-1$

$$\nabla_h^2 \overline{\omega} = \nabla_h^2 \omega_e + O(h^2) \parallel \psi_e \parallel_{C^6} . \tag{29}$$

Again by using Taylor expansion we get

$$\begin{aligned} \nabla_h^2 \omega_e &= \nabla^2 \omega_e + O(h^2) \parallel \omega_e \parallel_{C^4} \\ &= \nabla^2 \omega_e + O(h^2) \parallel \psi_e \parallel_{C^6} . \end{aligned} \tag{30}$$

Equations (29) and (30) lead to

$$\nabla_h^2 \overline{\omega} = \nabla^2 \omega_e + O(h^2) \parallel \psi_e \parallel_{C^6} . \tag{31}$$

For the unsteady term of the Stokes equation (20), we have

$$\begin{aligned} \frac{\partial \overline{\omega}}{\partial t} - \frac{\partial \omega_e}{\partial t} &= \frac{\partial}{\partial t}\nabla_h^2 \psi_e - \frac{\partial}{\partial t}\nabla^2 \psi_e \\ &= (\nabla_h^2 - \nabla^2)\frac{\partial \psi_e}{\partial t} \\ &= O(h^2)\left\| \frac{\partial \psi_e}{\partial t} \right\|_{C^4}. \end{aligned} \tag{32}$$

Following the work of Wang and Liu [19], it can be shown that

$$\begin{aligned} \left\| \frac{\partial \psi_e}{\partial t} \right\|_{C^{4,\alpha}} &\le C \left\| \frac{\partial \omega_e}{\partial t} \right\|_{C^{2,\alpha}} \\ &\le C \| \psi_e \|_{C^{6,\alpha}} \end{aligned} \tag{33}$$

for some $\alpha > 0$. Equations (32) and (33) together imply

$$\frac{\partial \overline{\omega}}{\partial t} - \frac{\partial \omega_e}{\partial t} = O(h^2) \| \psi_e \|_{C^{6,\alpha}}. \tag{34}$$

Finally combining Eqs. (31) and (34) we arrive at

$$\frac{\partial \overline{\omega}}{\partial t} = \frac{1}{Re}\nabla_h^2 \overline{\omega} + O(h^2) \| \psi_e \|_{C^{6,\alpha}}. \tag{35}$$

Next we proceed to show that the constructed $\overline{\omega}$ is consistent with the newly developed boundary conditions applied to $\overline{\psi}$. Using Taylor series expansion it is easy to see that

$$\frac{1}{h^2}(A_1 \overline{\psi}_{1,j} + A_2 \overline{\psi}_{2,j}) = \omega_e(0, y_j) + O(h) \| \psi_e \|_{C^3}. \tag{36}$$

Combining Eqs. (28) and (36) we get

$$\overline{\omega}_{0,j} = \frac{1}{h^2}(A_1 \overline{\psi}_{1,j} + A_2 \overline{\psi}_{2,j}) + O(h) \| \psi_e \|_{C^3} \tag{37}$$

which completes consistency analysis.

3.1.2 Stability Analysis

Theorem 3 *The numerical scheme* (21) *together with the vorticity boundary condition* (23) *is* L^2 *stable.*

Proof Considering inner product of Eq. (21) with ψ we have

$$\begin{aligned} \left\langle \psi, \frac{\partial \omega}{\partial t} \right\rangle &= \left\langle \psi, \frac{1}{Re} \nabla_h^2 \omega \right\rangle \\ \Rightarrow -\left\langle \psi, \frac{\partial}{\partial t} \nabla_h^2 \psi \right\rangle &= \frac{1}{Re} (\langle \nabla_h^2 \psi, \omega \rangle + \mathcal{BT}) \\ \Rightarrow \frac{Re}{2} \frac{d}{dt} \|\nabla_h \psi\|^2 &= -\|\omega\|^2 + \mathcal{BT} \end{aligned} \tag{38}$$

where $\mathcal{BT} = \mathcal{BT}_1 + \mathcal{BT}_2 + \mathcal{BT}_3 + \mathcal{BT}_4$ is the boundary term. We consider

$$\mathcal{BT}_1 = \sum_{j=1}^{N-1} \psi_{1,j} \omega_{0,j} \tag{39}$$

with similar expressions for $\mathcal{BT}_2, \mathcal{BT}_3, \mathcal{BT}_4$. The details of which may be found in [19,20]. As delineated by Wang and Liu [19] and Wang [20] we use the equivalent form Eq. (24) of the boundary condition Eq. (23) to bound the term $\mathcal{BT}$. Thus

$$\begin{aligned} \mathcal{BT}_1 &= \sum_{j=1}^{N-1} \left[B_1 \frac{\psi_{1,j}^2}{h^2} + B_2 \psi_{1,j} D_x^2 \psi_{1,j} \right] \\ &\leq \sum_{j=1}^{N-1} \left[B_1 \frac{\psi_{1,j}^2}{h^2} + B_2 \left(\frac{\psi_{1,j}}{2h} \right)^2 + B_2 \left(h D_x^2 \psi_{1,j} \right)^2 \right] \\ &= \sum_{j=1}^{N-1} \left[\left(B_1 + \frac{B_2}{4} \right) \frac{\psi_{1,j}^2}{h^2} + B_2 h^2 \left| D_x^2 \psi_{1,j} \right|^2 \right]. \end{aligned} \tag{40}$$

Using the values of A_1 and A_2 in the above inequality we finally arrive at

$$\mathcal{BT}_1 \leq \frac{h^2}{2} \sum_{j=1}^{N-1} \left| D_x^2 \psi_{1,j} \right|^2. \tag{41}$$

Proceeding similarly for $\mathcal{BT}_2$, $\mathcal{BT}_3$ and $\mathcal{BT}_4$ and adding we can show that

$$\begin{aligned} \mathcal{BT} &\leq \frac{1}{2} \left(\left\| D_x^2 \psi \right\|^2 + \left\| D_y^2 \psi \right\|^2 \right) \\ &\leq \frac{1}{2} \|\omega\|^2. \end{aligned} \tag{42}$$

The last inequality uses the following lemma established by Wang and Liu [19] and is reproduced here for completeness.

Lemma 1 *For any* ψ *such that* $\psi|_{\partial\Omega} = 0$,

$$\left\| D_x^2 \psi \right\|^2 + \left\| D_y^2 \psi \right\|^2 \leq \left\| \left(D_x^2 + D_y^2 \right) \psi \right\|^2 = \|\omega\|^2. \tag{43}$$

Using Eq. (42) in Eq. (38) we finally arrive at

$$Re\frac{d}{dt}\|\nabla_h\psi\|^2 + \|\omega\|^2 \leq 0. \tag{44}$$

This completes the stability analysis. □

3.1.3 Error Estimate

For $0 \leq i, j \leq N$, let us define

$$\widetilde{\psi}_{i,j} = \psi_{i,j} - \overline{\psi}_{i,j}, \quad \widetilde{\omega}_{i,j} = \omega_{i,j} - \overline{\omega}_{i,j}. \tag{45}$$

Subtracting Eq. (35) from Eq. (21), we have

$$\frac{\partial\widetilde{\omega}}{\partial t} = \frac{1}{Re}\nabla_h^2\widetilde{\omega} + F_1, \quad -\nabla_h^2\widetilde{\psi} = \widetilde{\omega}, \quad \widetilde{\psi}|_{\partial\Omega} = 0, \quad \left.\frac{\partial\widetilde{\psi}}{\partial\boldsymbol{n}}\right|_{\partial\Omega} = 0, \tag{46}$$

where $|F_1| \leq Ch^2\|\psi_e\|_{C^{6,\alpha}}$. From Eqs. (24) and (37) we have on the boundary

$$\widetilde{\omega}_{0,j} = \frac{1}{h^2}(A_1\widetilde{\psi}_{1,j} + A_2\widetilde{\psi}_{2,j}) + F_2. \tag{47}$$

with $F_2 \leq Ch\|\psi_e\|_{C^3}$. Taking inner product of vorticity error relation in Eq. (46) with $\widetilde{\psi}$ we get

$$\begin{aligned}
\left\langle\widetilde{\psi}, \frac{\partial\widetilde{\omega}}{\partial t}\right\rangle &= \left\langle\widetilde{\psi}, \frac{1}{Re}\nabla_h^2\widetilde{\omega}\right\rangle + \langle\widetilde{\psi}, F_1\rangle \\
\Rightarrow -\left\langle\widetilde{\psi}, \frac{\partial}{\partial t}\nabla_h^2\widetilde{\psi}\right\rangle &= \frac{1}{Re}(\langle\nabla_h^2\widetilde{\psi}, \widetilde{\omega}\rangle + \mathcal{BT}) + \langle\widetilde{\psi}, F_1\rangle \\
\Rightarrow \frac{1}{2}\frac{d}{dt}\|\nabla_h\widetilde{\psi}\|^2 &= \frac{1}{Re}(-\|\widetilde{\omega}\|^2 + \mathcal{BT}) + \langle\widetilde{\psi}, F_1\rangle
\end{aligned} \tag{48}$$

where $\mathcal{BT} = \mathcal{BT}_1 + \mathcal{BT}_2 + \mathcal{BT}_3 + \mathcal{BT}_4$ is the boundary term decomposed into four parts as earlier. We now proceed to bound $\mathcal{BT}$ in a manner similar to that of Sect. 3.1.2. Here,

$$\begin{aligned}
\mathcal{BT}_1 &= \sum_{j=1}^{N-1}\widetilde{\psi}_{1,j}\widetilde{\omega}_{0,j} \\
&= \sum_{j=1}^{N-1}\left[B_1\frac{\widetilde{\psi}_{1,j}^2}{h^2} + B_2\widetilde{\psi}_{1,j}D_x^2\widetilde{\psi}_{1,j} + \widetilde{\psi}_{1,j}F_2\right] \\
&\leq \sum_{j=1}^{N-1}\left[\left(B_1 + \frac{B_2}{4} + \frac{1}{2}\right)\frac{\widetilde{\psi}_{1,j}^2}{h^2} + B_2h^2\left|D_x^2\widetilde{\psi}_{1,j}\right|^2 + \frac{h^2}{2}|F_2|^2\right] \\
&\leq \sum_{j=1}^{N-1}\left[\frac{h^2}{2}\left|D_x^2\widetilde{\psi}_{1,j}\right|^2 + Ch^4\|\psi_e\|_{C^3}^2\right]
\end{aligned} \tag{49}$$

since $B_1 + \frac{B_2}{4} + \frac{1}{2} < 0$ and $0 \le B_2 < \frac{1}{2}$. Thus using $h = 1/N$ we arrive at

$$\begin{aligned}\mathcal{BT} &\le \frac{1}{2}\left(\left\|D_x^2\widetilde{\psi}\right\|^2 + \left\|D_y^2\widetilde{\psi}\right\|^2\right) + Ch^3\|\psi_e\|_{C^3}^2 \\ &\le \frac{1}{2}\|\widetilde{\omega}\|^2 + Ch^3\|\psi_e\|_{C^3}^2 \end{aligned} \tag{50}$$

where we have used the Lemma 1 [19] which also holds for $\widetilde{\psi}$. Also

$$|\langle\widetilde{\psi}, F_1\rangle| \le \frac{\|\widetilde{\psi}\|^2}{2} + \frac{\|F_1\|^2}{2}. \tag{51}$$

Using Eqs. (50) and (51) in Eq. (48) we get

$$\frac{d}{dt}\|\nabla_h\widetilde{\psi}\|^2 \le \|\widetilde{\psi}\|^2 - \frac{\|\widetilde{\omega}\|^2}{Re} + \|F_1\|^2 + Ch^3\|\psi_e\|_{C^3}^2. \tag{52}$$

Application of Poincare inequality for $\widetilde{\psi}$ implies

$$\frac{d}{dt}\|\nabla_h\widetilde{\psi}\|^2 \le C\|\nabla_h\widetilde{\psi}\|^2 - \frac{\|\widetilde{\omega}\|^2}{Re} + \|F_1\|^2 + Ch^3\|\psi_e\|_{C^3}^2. \tag{53}$$

Finally using Gronwall inequality to Eq. (53) we arrive at

$$\begin{aligned}\|\nabla_h\widetilde{\psi}\|^2 &\le e^{Ct}\int_0^t e^{-Ct}\left(-\frac{\|\widetilde{\omega}\|^2}{Re} + \|F_1\|^2 + Ch^3\|\psi_e\|_{C^3}^2\right)dt \\ \Rightarrow \|\nabla_h\widetilde{\psi}\|^2 + \frac{1}{Re}\int_0^t\|\widetilde{\omega}\|^2dt &\le Ce^{Ct}\int_0^t e^{-Ct}\left(h^4\|\psi_e\|_{C^{6,\alpha}}^2 + h^3\|\psi_e\|_{C^3}^2\right)dt. \end{aligned} \tag{54}$$

Hence

$$\|\nabla_h\widetilde{\psi}\| + \frac{1}{\sqrt{Re}}\left(\int_0^T\|\widetilde{\omega}\|^2dt\right)^{\frac{1}{2}} \le Ce^{CT}h^{\frac{3}{2}}\left(h^{\frac{1}{2}}\|\psi_e\|_{L^\infty([0,T],C^{6,\alpha})} + \|\psi_e\|_{L^\infty([0,T],C^3)}\right). \tag{55}$$

Thus we have established the following theorem:

Theorem 4 *Let $\psi_e \in L^\infty([0,T];C^{6,\alpha}(\overline{\Omega}))$, ω_e be the exact solution of the Stokes equation (20) and ψ_h, ω_h be the approximate solution of the numerical scheme Eq. (21) with vorticity boundary formula Eq. (23), then we have*

$$\begin{aligned}&\|\nabla_h(\psi_e - \psi_h)\|_{L^\infty([0,T],L^2)} + \frac{1}{\sqrt{Re}}\|\omega_e - \omega_h\|_{L^2([0,T],L^2)} \\ &\le Ce^{CT}h^{\frac{3}{2}}\left(h^{\frac{1}{2}}\|\psi_e\|_{L^\infty([0,T],C^{6,\alpha})} + \|\psi_e\|_{L^\infty([0,T],C^3)}\right). \end{aligned} \tag{56}$$

3.2 Comparison with Existing Local Boundary Conditions

Prior to the application of the four vorticity boundary conditions Eqs. (8)–(11) developed here, it is important to point out how these boundary conditions compare with the existing local boundary conditions. We also intend to highlight here the essential differences between the newly developed philosophy *vis-a-vis* some commonly used conditions. For totality we consider the following six boundary conditions.

1. Thom 1933 [6]:

$$\omega_{0,j} = \frac{2}{h^2}(\psi_{0,j} - \psi_{1,j} + h\psi_{x_{0,j}}) - \psi_{yy_{0,j}}. \tag{57}$$

2. Wilkes–Pearson 1965 [21]:

$$\omega_{0,j} = \frac{1}{2h^2}(7\psi_{0,j} - 8\psi_{1,j} + \psi_{2,j} + 6h\psi_{x_{0,j}}) - \psi_{yy_{0,j}}. \tag{58}$$

3. Orszag–Israeli 1974 [8]:

$$\omega_{0,j} = \frac{1}{13h^2}(34\psi_{0,j} - 35\psi_{1,j} + \psi_{3,j} + 32h\psi_{x_{0,j}}) - \psi_{yy_{0,j}}. \tag{59}$$

4. Briley 1971 [22]:

$$\omega_{0,j} = \frac{1}{18h^2}(85\psi_{0,j} - 108\psi_{1,j} + 27\psi_{2,j} - 4\psi_{3,j} + 66h\psi_{x_{0,j}}) - \psi_{yy_{0,j}}. \tag{60}$$

5. Woods 1954 [23]:

$$\omega_{0,j} = -\frac{1}{2}\omega_{1,j} + \frac{3}{h^2}(\psi_{0,j} - \psi_{1,j} + h\psi_{x_{0,j}}) - \frac{3}{2}\left(\psi_{yy_{0,j}} + \frac{h}{3}\psi_{xyy_{0,j}}\right). \tag{61}$$

6. D'Alessio–Dennis 1994 [24]:

$$\omega_{0,j} = -\frac{4}{3}\omega_{1,j} + \frac{1}{3}\omega_{2,j} + \frac{4}{h^2}(\psi_{0,j} - \psi_{1,j} + h\psi_{x_{0,j}}) - 2\left(\psi_{yy_{0,j}} + \frac{h}{3}\psi_{xyy_{0,j}}\right). \tag{62}$$

As noted in some of the previous works [5,14] all the above vorticity boundary conditions can be derived by exploiting the relationship between the vorticity and streamfunction *viz.* the elliptic vorticity equation (2) at the left boundary. In case of partial differential equations the boundary conditions and the initial conditions are as significant as that of the governing equation in computing the solution. It is quite elegant to incorporate both the boundary condition and the governing equations to derive the boundary discretization formula. Also judging from the fact that one can obtain reasonable results with some of these schemes, they continue to be popular in the computational fluid dynamics community [25,26], we can infer that they must implicitly satisfy some specific vorticity boundary requirements. One of the motivations of this work is also to shed some light on this issue as well. Specifically in this work we make use of vorticity integral condition Eq. (6) which is applicable on the boundary and also explore it *vis-a-vis* well known vorticity boundary conditions.

Using Taylor series expansion we see that the Thom's condition Eq. (57) reduces to

$$\omega_{0,j} = -(\psi_{xx_{0,j}} + \psi_{yy_{0,j}}) + O(h).$$

This indicates that it is a first order accurate approximation of Eq. (2) at the point $(0, j)$. But this first order accuracy for the Thom's formula is often misleading as can be clearly seen from the numerical and analytical works presented in [4,5,7]. As will be seen later in Sect. 4 there is a close correspondence between the results produced by the newly developed formula Eq. (8) and the Thom's condition Eq. (57). Thus we shall like to investigate them in more details.

Consider a numerical scheme which uses second order central differencing to estimate normal derivatives at grid points adjacent to the boundary *viz.*, $\psi_{xx_{1,j}} = (\psi_{0,j} - 2\psi_{1,j} + \psi_{2,j})/h^2$ and $\psi_{x_{1,j}} = (\psi_{2,j} - \psi_{0,j})/2h$. These approximations employed in the formula Eq. (8) yield

$$\omega_{0,j} = \frac{2}{h^2}(\psi_{0,j} - \psi_{1,j} + h\psi_{x_{0,j}}) - \frac{1}{2k}(\psi_{y_{0,j+1}} - \psi_{y_{0,j-1}}) + \left[\psi_{yy_{1,j}} - \frac{1}{2k}(\psi_{y_{1,j+1}} - \psi_{y_{1,j-1}})\right].$$

Although a detailed analysis may be necessary but a second order estimate of $\psi_{yy_{i,j}}$ by $(\psi_{y_{i,j+1}} - \psi_{y_{i,j-1}})/2k$ reveals that for any numerical scheme the Eq. (8) approaches Thom's condition Eq. (57) and as such it should not be surprising if the results are comparable. Of course for computational methods using higher order discretization at interior grid points the results obtained by Eqs. (8) and (57) are expected to differ on the boundaries as the boundary condition *New 1* will be different from Thom's condition.

Again Taylor expansion renders both the Wilkes–Pearson's condition Eq. (58) and the Orszag–Israeli condition Eq. (59) to reduce to second order approximation

$$\omega_{0,j} = -(\psi_{xx_{0,j}} + \psi_{yy_{0,j}}) + O(h^2)$$

of the Eq. (2); whereas the Briley Eq. (60) gives still higher third order accurate approximation of the same equation at the left boundary. Orszag and Israeli [8] originally designed formulation for the homogeneous boundary condition by matching the eigenvalues of finite difference approximation with the exact one for unsteady Stokes equation. The scheme presented here is an extension of the same for the inhomogeneous problem. With the vorticity integral condition Eq. (6), the success of the four boundary conditions Eqs. (57)–(60) may be ascribed as an approximation of the equation

$$\omega_{\epsilon,j} 2\epsilon hk = \psi_{x_{0,j}} k - \psi_{x_{2\epsilon,j}} k + \psi_{y_{\epsilon,j-1/2}} 2\epsilon h - \psi_{y_{\epsilon,j+1/2}} 2\epsilon h \tag{63}$$

with ϵ being taken to be a small number. Equation (63) is the completion of the Eq. (6) with a cell of length 2ϵ.

We now proceed to the remaining two boundary conditions given by Wood [23] and D'Alessio and Dennis [24]. It is interesting to note that the Taylor series expansions of the Wood's boundary condition Eq. (61) and D'Alessio–Dennis Eq. (62) yield

$$\omega_{1/3,j} = -(\psi_{xx_{1/3,j}} + \psi_{yy_{1/3,j}}) + O(h^2)$$

with the leading error terms $\frac{h^2}{12}(2\omega_{xx_{1/3,j}} - \psi_{xxxx_{1/3,j}})$ and $-\frac{h^2}{12}\psi_{xxxx_{1/3,j}}$, respectively. Making use of the relations

$$\frac{3}{2h}(\psi_{x_{0,j}} - \psi_{x_{2/3,j}}) = \frac{2}{h^2}(\psi_{0,j} - \psi_{1,j} + h\psi_{x_{0,j}}) + O(h^2)$$

and

$$\frac{1}{k}(\psi_{y_{1/3,j+1/2}} - \psi_{y_{1/3,j-1/2}}) = \psi_{yy_{0,j}} + \frac{h}{3}\psi_{xyy_{0,j}} + O(h^2, k^2)$$

we see that Eqs. (61) and (62) can be conceptualized as

$$\omega_{1/3,j}\frac{2h}{3}k = \psi_{x_{0,j}} k - \psi_{x_{2/3,j}} k + \psi_{y_{1/3,j-1/2}}\frac{2h}{3} - \psi_{y_{1/3,j+1/2}}\frac{2h}{3}. \tag{64}$$

Equation (64) is the identical particular form of the vorticity integral condition Eq. (6) from which Eq. (9) was deduced by using a different discretization procedure. Although Eq. (9) is of first order accuracy but Eqs. (61) and (62) are second order implementations albeit with different associated error terms.

4 Results and Discussion

4.1 Problem 1: A Model Problem for Unsteady Incompressible Flow

We first implement the vorticity integral condition given by the Eq. (6) for the unsteady two dimensional Stokes equation (20) in a domain $[-1, 1] \times [0, 2\pi]$. The problem contemplated is a two-dimensional linear model which satisfies the no-slip boundary condition in the x-direction and the periodic boundary condition along the y-direction and admits exact solution

$$u(x, y, t) = \hat{u}(x)e^{Iy+\sigma t}, \quad v(x, y, t) = \hat{v}(x)e^{Iy+\sigma t}, \quad p(x, y, t) = \hat{p}(x)e^{Iy+\sigma t}$$

where $I = \sqrt{-1}$. This model exemplifies the essential features of the incompressibility and viscosity of the Navier–Stokes equations [4,27]. In terms of vorticity and streamfunction the exact solution is

$$\omega = I\left(\frac{d^2\hat{u}}{dx^2}(x) - \hat{u}(x)\right)e^{Iy+\sigma t}, \quad \psi = -I\hat{u}(x)e^{Iy+\sigma t}.$$

We consider the antisymmetric exact solution corresponding to

$$\hat{u}(x) = \sin\mu\frac{\sinh x}{\sinh 1} - \sin\mu x$$

with $\mu = 4.423863790876$ and $\sigma = -\nu(\mu^2 + 1)$, ν being the kinematic viscosity.

The system of equations in Eq. (20) is discretized by using the standard second order central difference operators as far as the space derivatives are concerned. For the time derivative implicit Crank–Nicolson has been employed. We solve the flow in a grid of size 64×199 with a time step 0.001 for $Re = 100$. A small time step has been considered to reduce the influence of time discretization. We carry out computations for all the ten vorticity boundary conditions discussed earlier. In the Fig. 2a the difference between the real part of exact and computed vorticity values has been plotted along the line $y = \frac{\pi}{4}$ at time $t = 1.0$. In this figure we see that the newly developed vorticity boundary condition given by the Eq. (8) executes exactly similar to that of Thom formula Eq. (57). Here the second boundary condition Eq. (9) performs better. All the remaining boundary conditions demonstrate better execution. To get an enhanced idea of the remaining boundary conditions we plot a closeup view in the Fig. 2b. Although the results are comparable clearly the boundary condition given in Eq. (10) shows better accuracy compared to the other ones. What is interesting to note is that the boundary condition developed by considering cell center at $x = \frac{1}{16}$ given by Eq. (11) yields a less accurate solution at the boundary compared to the condition developed by taking cell center at $x = \frac{1}{4}$. This may be attributed to the associated truncation error. Also the schemes of Orszag–Israeli Eq. (59) and D'Alessio–Dennis Eq. (62) perform well. As it has been noted earlier the scheme due to D'Alessio and Dennis can be interpreted as adhering to

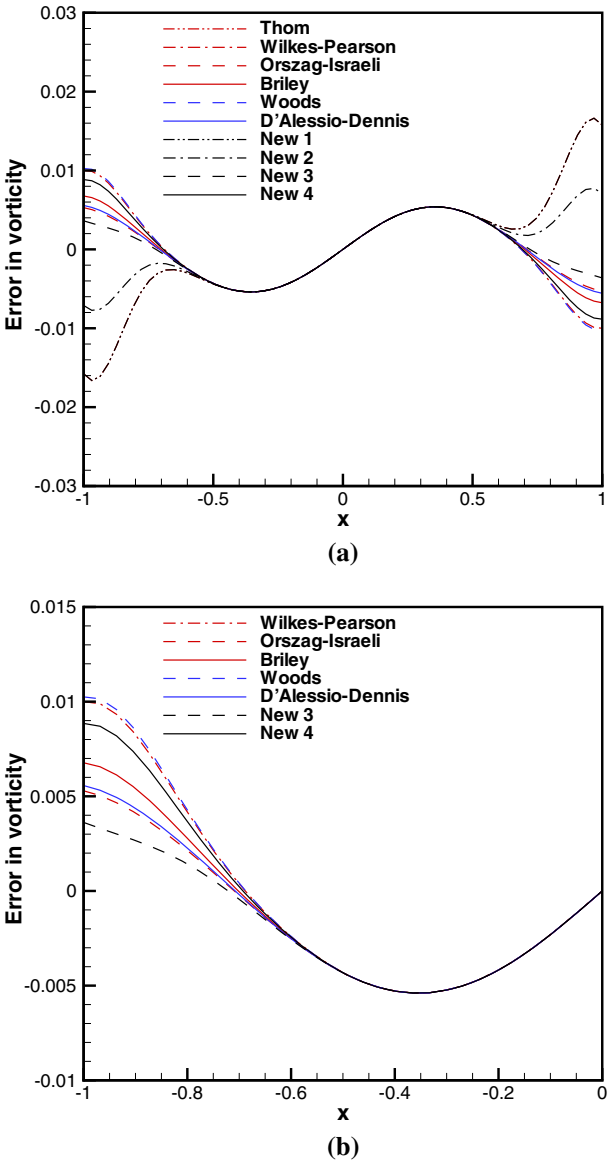

Fig. 2 Problem 1: Error in the real part of the exact and computed vorticity values along the line $y = \frac{\pi}{4}$ at time $t = 1.0$. **a** Full view, **b** closeup view

the philosophy expressed by the Eq. (6) whereas the scheme of Orszag and Israeli has been specifically developed for the particular type of problem investigated here.

4.2 Problem 2: A Problem with Analytic Solution for Steady Stokes Equation

To verify the order of accuracy of the different boundary conditions we cogitate the steady state form of the Stokes system Eq. (20) in a unit square domain $\Omega = [0, 1]^2$. The problem

Table 1 Problem 2: $G.R.E.$ in steady state ω field

	49×49	Order	97×97	Order	193×193
Thom [6]	6.062×10^{-4}	2.03	1.487×10^{-4}	2.02	3.655×10^{-5}
Wilkes–Pearson [21]	1.093×10^{-4}	2.10	2.541×10^{-5}	2.06	6.102×10^{-6}
Orszag–Israeli [8]	1.797×10^{-4}	2.11	4.166×10^{-5}	2.07	9.925×10^{-6}
Briley [22]	1.120×10^{-4}	2.12	2.579×10^{-5}	2.07	6.151×10^{-6}
Woods [23]	1.128×10^{-4}	2.12	2.590×10^{-5}	2.07	6.164×10^{-6}
D'Alessio–Dennis [24]	1.132×10^{-4}	2.13	2.594×10^{-5}	2.07	6.169×10^{-6}
New 1, Eq. (8)	6.064×10^{-4}	2.03	1.488×10^{-4}	2.03	3.655×10^{-5}
New 2, Eq. (9)	4.150×10^{-4}	2.05	1.005×10^{-4}	2.04	2.451×10^{-5}
New 3, Eq. (10)	1.792×10^{-4}	2.21	4.162×10^{-5}	1.96	9.920×10^{-6}
New 4, Eq. (11)	1.069×10^{-4}	2.12	2.466×10^{-5}	2.07	5.880×10^{-6}

Comparison of results obtained using different boundary conditions

Table 2 Problem 2: $G.R.E.$ in steady state ψ field

	49×49	Order	97×97	Order	193×193
Thom [6]	2.220×10^{-5}	1.96	5.690×10^{-6}	1.98	1.440×10^{-6}
Wilkes–Pearson [21]	2.236×10^{-7}	3.34	2.202×10^{-8}	1.68	6.858×10^{-9}
Orszag–Israeli [8]	5.766×10^{-6}	2.00	1.439×10^{-6}	2.00	3.593×10^{-7}
Briley [22]	1.013×10^{-7}	1.56	3.443×10^{-8}	1.75	1.022×10^{-8}
Woods [23]	1.856×10^{-7}	2.03	4.536×10^{-8}	1.97	1.157×10^{-8}
D'Alessio–Dennis [24]	1.829×10^{-7}	1.95	4.715×10^{-8}	1.98	1.195×10^{-8}
New 1, Eq. (8)	2.183×10^{-5}	1.95	5.642×10^{-6}	1.97	1.434×10^{-6}
New 2, Eq. (9)	1.485×10^{-5}	1.96	3.795×10^{-6}	1.98	9.589×10^{-7}
New 3, Eq. (10)	5.664×10^{-6}	1.98	1.426×10^{-6}	1.99	3.577×10^{-7}
New 4, Eq. (11)	1.158×10^{-6}	2.13	2.637×10^{-7}	2.07	6.286×10^{-8}

Comparison of results obtained using different boundary conditions

admits an analytical solution given by $\omega = 2e^x \sin y$, $\psi = -xe^x \sin y$ [5]. The boundary conditions $\psi|_{\partial\Omega}$ and $\frac{\partial\psi}{\partial \boldsymbol{n}}\big|_{\partial\Omega}$ can be obtained from the analytical solution. Here again we consider second order discretization and compute solutions in three different uniform grids *viz.* 49×49, 97×97 and 193×193. Note that the steady system of equations contemplated here is coupled via boundary conditions which are provided only for streamfunction and its normal gradient. In our calculations we demand the residual be less than 10^{-10} and assume that the steady state has been reached if difference between two successive iterations happens to be less than 10^{-15}. Following Napolitano *et al.* [5] we define the general relative error in computing $u(x, y)$ as:

$$G.R.E.(u) = \frac{\|u^c - u^e\|_{L^1}}{\|u^e\|_{L^1}}$$

Table 3 Problem 2: $B.R.E.$ in steady state boundary ω values

	49×49	Order	97×97	Order	193×193
Thom [6]	1.855×10^{-3}	1.71	5.679×10^{-4}	1.75	1.687×10^{-4}
Wilkes–Pearson [21]	8.766×10^{-5}	1.97	2.243×10^{-5}	1.97	5.708×10^{-6}
Orszag–Israeli [8]	5.080×10^{-4}	1.73	1.522×10^{-4}	1.77	4.457×10^{-5}
Briley [22]	9.082×10^{-5}	1.98	2.299×10^{-5}	1.99	5.796×10^{-6}
Woods [23]	9.288×10^{-5}	1.99	2.328×10^{-5}	1.99	5.838×10^{-6}
D'Alessio–Dennis [24]	9.357×10^{-5}	2.00	2.339×10^{-5}	2.00	5.841×10^{-6}
New 1, Eq. (8)	1.791×10^{-3}	1.70	5.507×10^{-4}	1.75	1.642×10^{-4}
New 2, Eq. (9)	1.284×10^{-3}	1.71	3.904×10^{-4}	1.76	1.154×10^{-4}
New 3, Eq. (10)	5.139×10^{-4}	1.73	1.540×10^{-4}	1.77	4.507×10^{-5}
New 4, Eq. (11)	1.335×10^{-4}	1.82	3.785×10^{-5}	1.83	1.063×10^{-5}

Comparison of results obtained using different boundary conditions

where u^c and u^e denote the computed and exact solutions. Similarly boundary relative error $B.R.E.(u)$ is defined as:

$$B.R.E.(u) = \frac{\|u_b^c - u_b^e\|_{L^1}}{\|u_b^e\|_{L^1}}$$

where u_b^c and u_b^e denote the computed and exact solutions at the boundary points only. $G.R.E.(\omega)$ and $G.R.E.(\psi)$ have been shown in the Tables 1 and 2, respectively. From these tables it is clear that all the formulations show second order of convergence irrespective of theoretical orders. Although the new formulation Eq. (11) is able to produce the lowest error for all the grids as far as the ω field is concerned but for computed ψ field error is the lowest with Wilkes–Pearson's method [21]. From the Table 3 we see that as far as the $B.R.E.(\omega)$ is concerned all methods show different orders of convergence. Finally in the Fig. 3a, b we present the computed difference between the exact and numerical vorticity values along the horizontal center line. As was earlier observed in Problem 1, here also we see that the boundary condition given by Eq. (8) performs exactly similar to that of Thom's formula Eq. (57) and the second boundary condition Eq. (9) performs marginally better than these two. A zoomed view provided in Fig. 3b suggests that overall the fourth boundary condition Eq. (11) is better than other boundary conditions. Here we see that the boundary condition due to Orszag and Israeli [8] produces less accuracy and is clustered with the result produced by Woods [23]. All the other schemes seem to produce little bit better results and are clustered together. Note that the approach of Woods [23] given by Eq. (60) and the approach of D'Alessio and Dennis [24] given in Eq. (61) provide much lesser errors than those obtained using Eq. (9). This result can be explained in the light of our earlier observations in Sect. 3.2 that Eqs. (60) and (61) are indeed second order implementations of the new vorticity integral condition Eq. (6).

We choose the following three canonical problems to validate the new boundary condition for flows governed by incompressible N–S equations. Apart from comparing the streamfunction and vorticity fields we also look forward to analyzing the pressure contours calculated directly using the streamfunction and vorticity values.

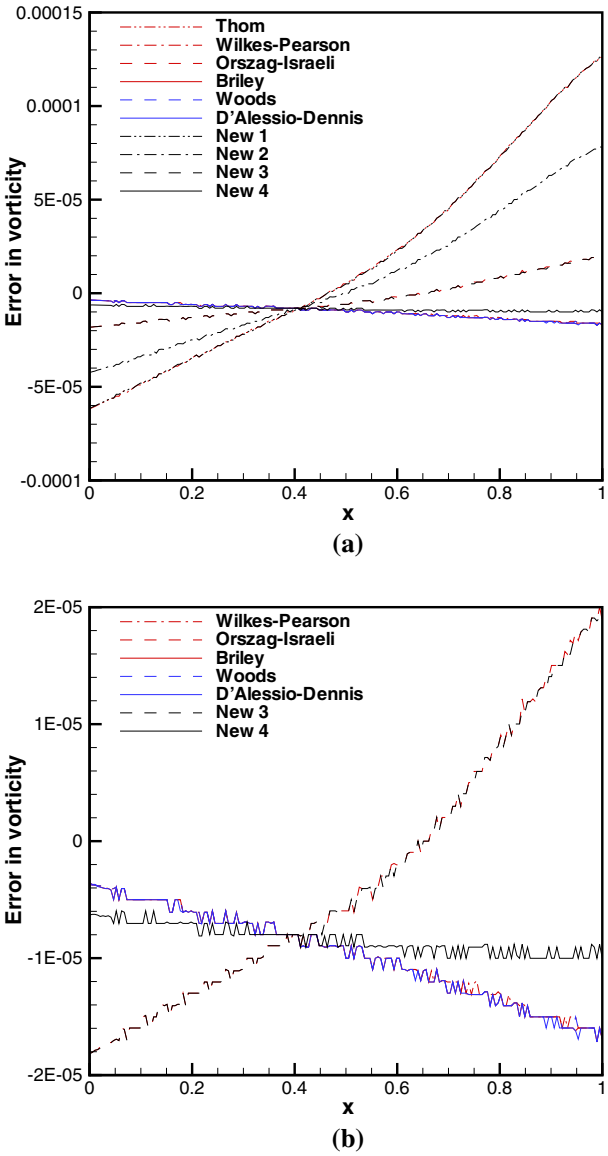

Fig. 3 Problem 2: Difference between the exact and computed vorticity values along the horizontal center line at steady state. **a** Full view, **b** closeup view

4.3 Problem 3: Lid Driven Cavity Flow

We present here the computed solutions for $Re = 100, 1000, 5000$ and $10,000$. For $Re = 100$, the solution is computed separately using a 65×65 grid with the newly developed boundary conditions Eqs. (8), (9), (10) and (11). For the sake of comparison we have also computed using Thom [6], Wilkes–Pearson [21], Orszag–Israli [8], Briley [22] and Woods [23] boundary conditions. The boundary condition D'Alessio–Dennis [24] has not been considered

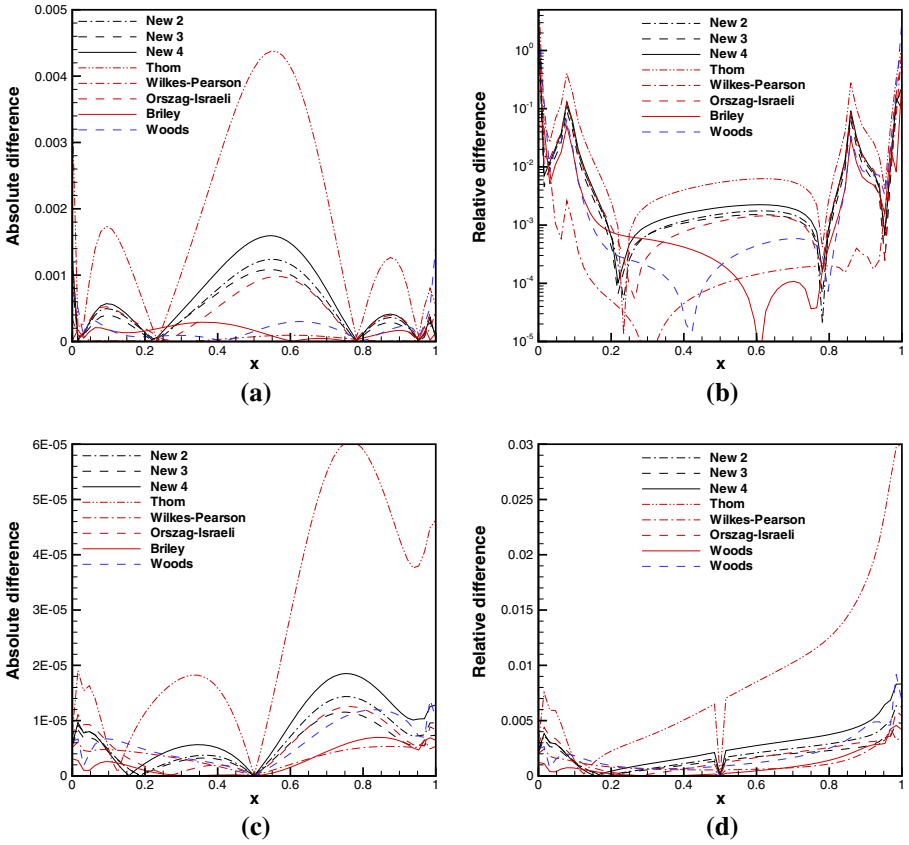

Fig. 4 Problem 3: Absolute and relative difference in vorticity and total pressure computed using different boundary conditions with respect to the solution computed using the boundary condition Eq. (8) at the bottom wall for $Re = 100$. **a** Absolute difference in vorticity. **b** Relative difference in vorticity. **c** Absolute difference in total pressure. **d** Relative difference in total pressure

as it uses a non compact stencil for vorticity and our computations are being carried out with a fourth order compact formulation [15]. Absolute and relative differences in vorticity at the bottom wall are presented in Fig. 4a, b, respectively. In the absence of analytical solution the above mentioned absolute and relative differences have been calculated with reference to the solution obtained using boundary condition Eq. (8). Similarly the absolute and relative differences in total pressure at the bottom wall are presented in Fig. 4c, d, respectively. We repeat the above computations for the right boundary in the Fig. 5. From these figures it is seen that as we resort to higher order compact discretization for derivatives, maximum difference is recorded with respect to the Thom formula [6] and is followed by *New 4* in both absolute and relative terms. Here it should be noted that for previous two problems results obtained by *New 1* and Thom were similar since all the derivatives were discretized by using second order central differences and is in conformity with our theoretical analysis. Overall pattern is similar for all the newly developed boundary conditions and the boundary condition of Orszag–Israeli [8]. From Fig. 4 it can be seen that for both vorticity and pressure at the bottom wall, differences between values computed using the boundary conditions *New 1*, Eq. (8) and Wilkes–Pearson [21] is much less. The same holds

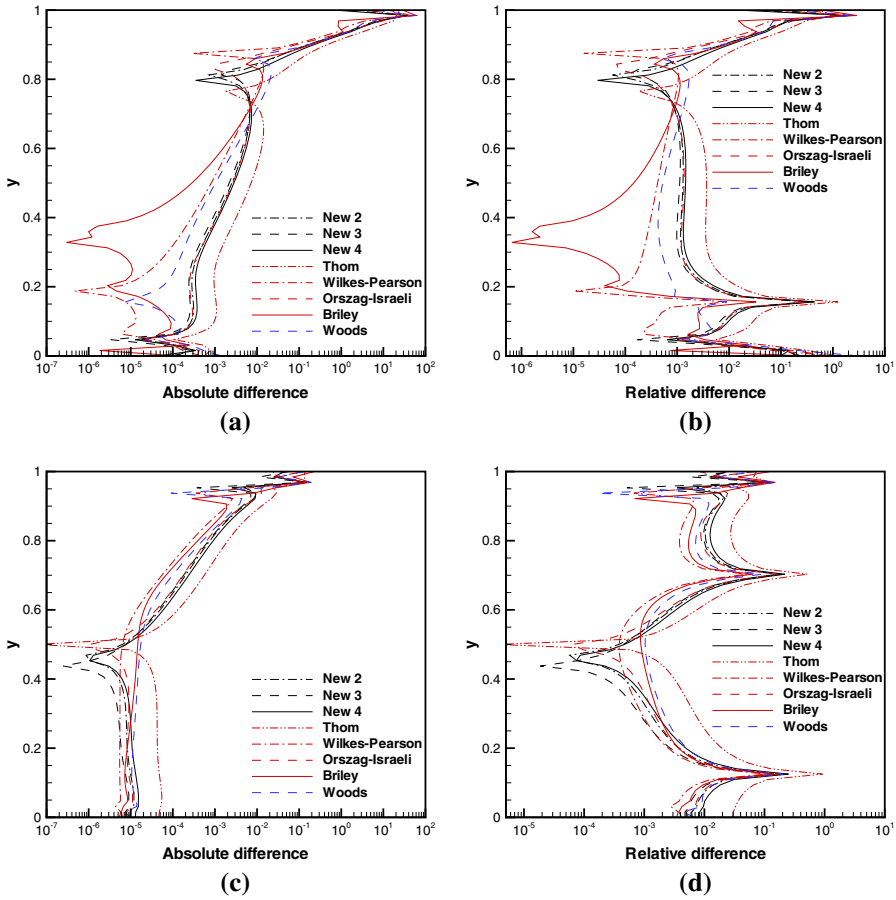

Fig. 5 Problem 3: Absolute and relative difference in vorticity and total pressure computed using different boundary conditions with respect to the solution computed using boundary condition Eq. (8) at the right wall for $Re = 100$. **a** Absolute difference in vorticity. **b** Relative difference in vorticity. **c** Absolute difference in total pressure. **d** Relative difference in total pressure

for Briley's [22] condition to a large extent. In the absence of singularity the maximum difference in both absolute and relative terms lies within the extremities for the bottom of the cavity as seen in Fig. 4. But the presence of singularity introduces maximum error at the top right corner and is evident from the Fig. 5. Next in Table 4 we present properties of primary, secondary and tertiary vortices for this problem for $Re = 100$ and 5000. For $Re = 5000$ the solution has been computed using 129×129 grid. Here results have been obtained using above mentioned nine different boundary conditions in conjunction with the scheme developed in [15]. The findings have been compared with the benchmark result of Ghia et al. [28]. Comparison with other benchmark results available in the literature has been avoided as the numerical solution is reliant on the scheme being used apart from boundary treatment. Although in our computation the scheme is identical we can observe differences in the strengths of the vortices with the variation in the boundary condition implementation. This table establishes the importance of correct boundary condition in accurate simulation of incompressible flow. The solvability condition presented in Eq. (4) is of funda-

Table 4 Problem 3: Properties of the primary, secondary and tertiary vortices for the lid-driven square cavity for $Re = 100$ and $Re = 5000$

Vortex	$Re = 100$	$Re = 5000$	Boundary condition/reference
Primary	ψ_{min}	ψ_{min}	
	-0.103532	-0.122755	New 1 (8)
	-0.103500	-0.122697	New 2 (9)
	-0.103499	-0.122694	New 3 (10)
	-0.103484	-0.122580	New 4 (11)
	-0.103427	-0.122069	Thom [6]
	-0.103535	-0.123356	Wilkes–Pearson [21]
	-0.103524	-0.123326	Orszag–Israeli [8]
	-0.103499	-0.122619	Briley [22]
	-0.103517	-0.122718	Woods [23]
	-0.103423	-0.118966	Ghia et al. [28]
Secondary	ψ_{max}	ψ_{max}	
TL	–	1.49634×10^{-3}	New 1 (8)
	–	1.53096×10^{-3}	New 2 (9)
	–	1.52320×10^{-3}	New 3 (10)
	–	1.53229×10^{-3}	New 4 (11)
	–	1.60083×10^{-3}	Thom [6]
	–	1.51372×10^{-3}	Wilkes–Pearson [21]
	–	1.55492×10^{-3}	Orszag–Israeli [8]
	–	1.47458×10^{-3}	Briley [22]
	–	1.48979×10^{-3}	Woods [23]
	–	1.45641×10^{-3}	Ghia et al. [28]
Secondary	ψ_{max}	ψ_{max}	
BL	1.81582×10^{-6}	1.39069×10^{-3}	New 1 (8)
	2.03833×10^{-6}	1.40455×10^{-3}	New 2 (9)
	1.99225×10^{-6}	1.39742×10^{-3}	New 3 (10)
	2.06675×10^{-6}	1.40557×10^{-3}	New 4 (11)
	2.60324×10^{-6}	1.42606×10^{-3}	Thom [6]
	1.82818×10^{-6}	1.40607×10^{-3}	Wilkes–Pearson [21]
	2.07410×10^{-6}	1.41897×10^{-3}	Orszag–Israeli [8]
	1.72088×10^{-6}	1.38859×10^{-3}	Briley [22]
	1.69788×10^{-6}	1.39032×10^{-3}	Woods [23]
	1.74877×10^{-6}	1.36119×10^{-3}	Ghia et al. [28]
Secondary	ψ_{max}	ψ_{max}	
BR	1.26848×10^{-5}	3.09818×10^{-3}	New 1 (8)
	1.35258×10^{-5}	3.13662×10^{-3}	New 2 (9)
	1.33691×10^{-5}	3.13638×10^{-3}	New 3 (10)
	1.36647×10^{-5}	3.15017×10^{-3}	New 4 (11)
	1.15849×10^{-5}	3.25299×10^{-3}	Thom [6]

Table 4 continued

Vortex	$Re = 100$	$Re = 5000$	Boundary condition/reference
	1.26952×10^{-5}	3.11696×10^{-3}	Wilkes–Pearson [21]
	1.35566×10^{-5}	3.16957×10^{-3}	Orszag–Israeli [8]
	1.24492×10^{-5}	3.07721×10^{-3}	Briley [22]
	1.24208×10^{-5}	3.09243×10^{-3}	Woods [23]
	1.25374×10^{-5}	3.08358×10^{-3}	Ghia et al. [28]
Tertiary	ψ_{min}	ψ_{min}	
BR	–	-1.50447×10^{-6}	New 1 (8)
	–	-1.80420×10^{-6}	New 2 (9)
	–	-1.73974×10^{-6}	New 3 (10)
	–	-1.86192×10^{-6}	New 4 (11)
	–	-3.06109×10^{-6}	Thom [6]
	–	-1.55771×10^{-6}	Wilkes–Pearson [21]
	–	-1.96847×10^{-6}	Orszag–Israeli [8]
	–	-1.38191×10^{-6}	Briley [22]
	–	-1.41558×10^{-6}	Woods [23]
	–	-1.43226×10^{-6}	Ghia et al. [28]
Grid size	65×65	129×129	Present computation
	129×129	257×257	Ghia et al. [28]

Table 5 Problem 3: Error extent to which solvability condition Eq. (4) has been satisfied for $Re = 100$ and 5000

Boundary condition	$Re = 100$	$Re = 5000$
Thom [6]	0.00922	0.00525
Wilkes–Pearson [21]	0.00439	0.00070
Orszag–Israeli [8]	0.00378	0.00318
Briley [22]	0.00577	0.00904
Woods [23]	0.00719	0.00431
New 1, Eq. (8)	0.00242	0.00540
New 2, Eq. (9)	0.00373	0.00106
New 3, Eq. (10)	0.00414	0.00268
New 4, Eq. (11)	0.00455	0.00401

mental importance in $\psi - \omega$ formulation and it has to be taken into account properly by any approach dealing with vorticity boundary condition. Table 5 we present the extent of absolute error to which this solvability condition has been satisfied at the steady state reached using the four newly developed vorticity conditions as well as other boundary conditions for $Re = 100$ and 5000. It is hearting to see that all the newly developed conditions perform well and produce relatively less error for $Re = 100$. For $Re = 5000$ the conditions *New 2* and *New 3* satisfy solvability condition to a large extent but Wilkes–Pearson [21] shows least error. This clearly establishes inherent potential of some of the well known vorticity boundary conditions. Finally we present streamline, vorticity and static pressure

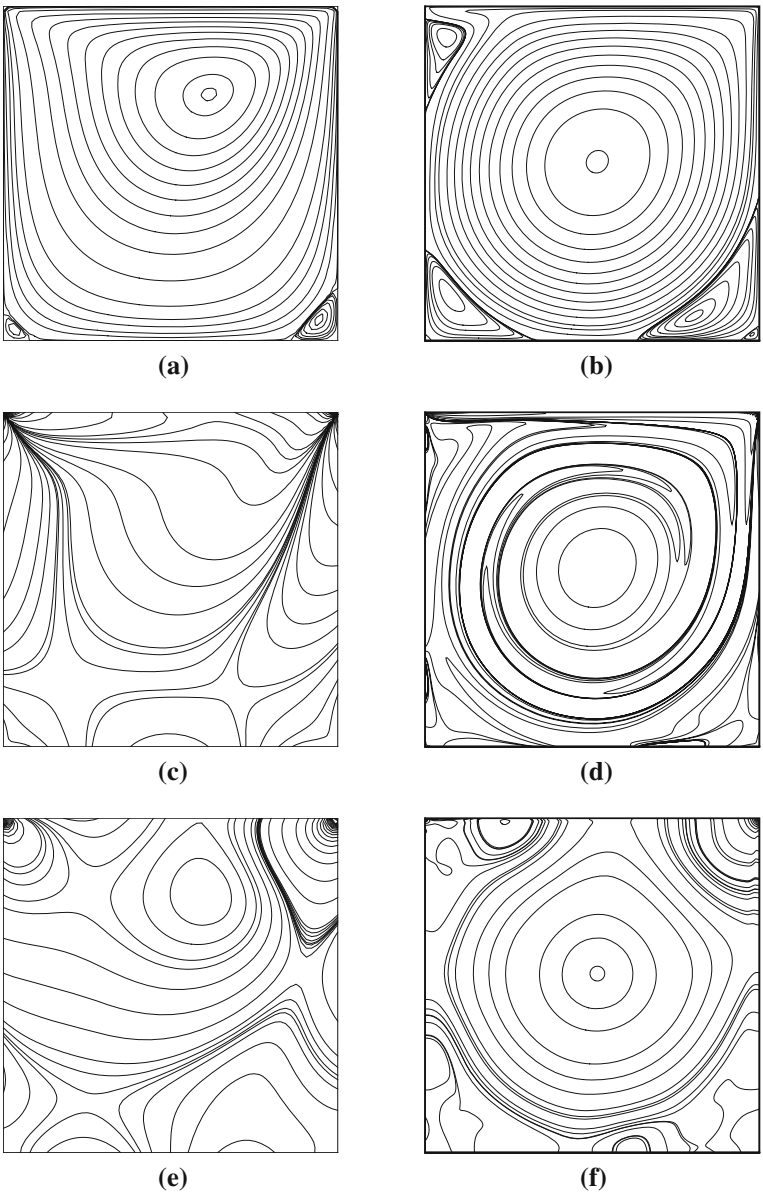

Fig. 6 Problem 3: Results for $Re = 100$ computed using 65×65 grid (*left*) and $Re = 5000$ computed using 257×257 grid (*right*). **a**, **b** Streamfunction. **c**, **d** Vorticity. **e**, **f** Static pressure

contours in Fig. 6 for $Re = 100$ and 5000 computed using the boundary condition Eq. (11).

We compare convergence behavior of the four newly developed boundary conditions given by the Eqs. (8), (9), (10), (11) with other established boundary conditions in Figs. 7 and 8. Corresponding relative CPU times have been charted in Table 6. In Figs. 7a and 8a convergence history corresponding to the first time step for $Re = 100$ and $Re = 1000$,

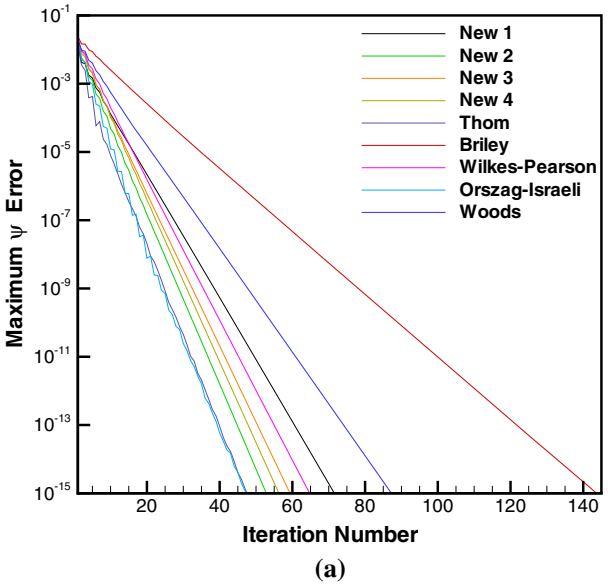

Fig. 7 Problem 3: Convergence history corresponding to $Re = 100$ for **a** first time step using unsteady code, **b** steady code

respectively, have been portrayed. These figures depict max- norm correction in stream-function field with respect to each inner iteration starting with zero initial condition for ψ. For $Re = 100$ it is seen that amongst the newly developed conditions *New 2* takes the least number of iteration whereas the formula *New 1* takes the greatest number of iterations and hence relative CPU time as seen in Table 6. Overall boundary condition of Thom [6] and Orszag–Israeli [8] are found to be best whereas Briley [22] and Woods [23] condi-

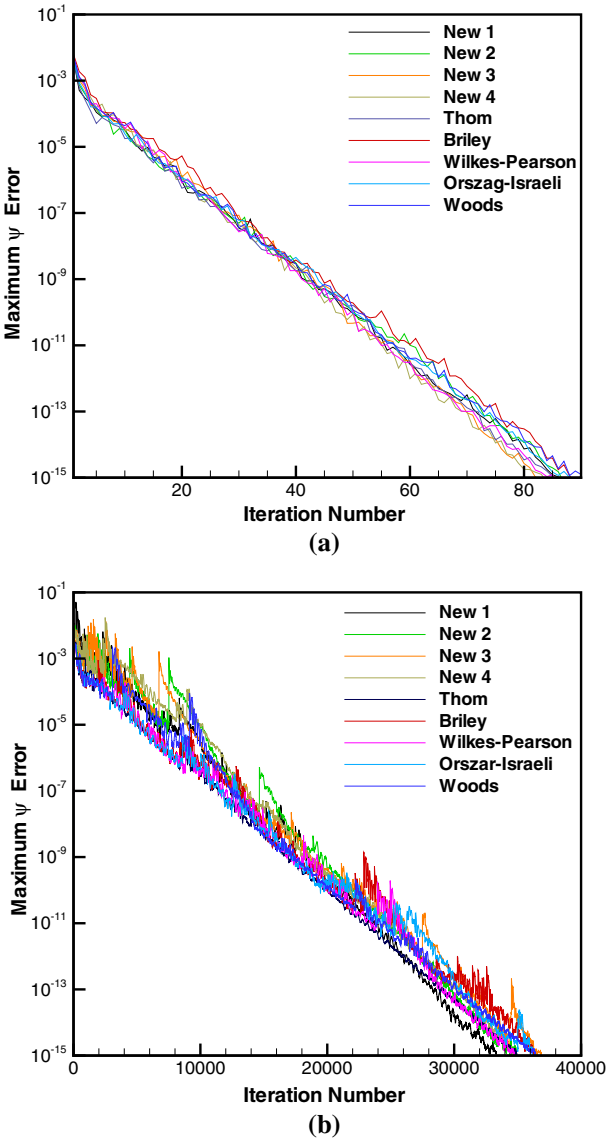

Fig. 8 Problem 3: Convergence history corresponding to $Re = 1000$ for **a** first time step using unsteady code, **b** steady code

tions lag behind. For $Re = 1000$ the formula *New 1* takes the highest number of iterations among the newly developed ones but here the difference between the number of iterations taken by different schemes is less. A slightly higher CPU time consumption is reported in Table 6 for *New 2 vis-a-vis New 1* boundary condition. This may be attributed to higher computational complexity involved in each iteration of *New 2*. We have also developed steady code for the lid driven cavity problem in conjunction with all the boundary conditions. The codes thus developed have been tested and convergence histories corresponding to different boundary conditions have been shown in Figs. 7b and 8b for $Re = 100$ and

Table 6 Problem 3: CPU-time comparison for various boundary conditions (relative values with New 1 as reference) in four different cases

Boundary condition	$Re = 100$		$Re = 1000$	
	Unsteady (1st time step)	Steady	Unsteady (1st time step)	Steady
New 1, Eq. (8)	1.0	1.0	1.0	1.0
New 2, Eq. (9)	0.767	0.995	1.003	1.047
New 3, Eq. (10)	0.870	1.035	0.957	1.499
New 4, Eq. (11)	0.913	1.028	0.967	1.043
Thom [6]	0.654	1.179	0.998	0.999
Briley [22]	1.973	1.097	1.027	1.090
Wilkes–Pearson [21]	0.908	1.125	1.003	1.046
Orszag–Israeli [8]	0.625	1.151	1.014	1.083
Woods [23]	1.276	1.098	1.012	1.093

$Re = 1000$, respectively. Here figures depict max- norm correction in streamfunction field with respect to each iteration till the steady state has been reached. For the steady problem it can be said that overall *New 1* performs best for both the Re values and is closely followed by the conditions *New 2* and *New 4*. From Table 6 one can infer that for both the steady cases CPU times consumed by the newly developed boundary conditions are less than those accounted for the established boundary conditions with the exception of *New 3* applied to $Re = 1000$.

Finally we compute with $Re = 10{,}000$ where an unsteady periodic flow is expected. We carry out our simulation using 129×129 grid with newly developed boundary conditions Eqs. (8) and (11). For both the boundary conditions an eventual periodic state with time period 1.65 has been found. In Fig. 9a we present the error extent of the solvability condition Eq. (4) for the entire period. From the figure it is clear that error is much lower for the boundary condition Eq. (11) as compared to boundary condition Eq. (8). In Fig. 9b we present the phase portrait of u and v velocities which establishes the periodic nature. Streamlines and total pressure contours at periodic state obtained using Eq. (8) have been presented in Figs. 10a and 10b, respectively. Whereas the results obtained via Eq. (11) at corresponding time can be found in Figs. 10c and 10d, respectively. A vorticity resolution check is carried out in Fig. 11 for $Re = 10{,}000$. In this figure we have depicted vorticity contours computed using two fine grids 257×257 and 513×513. It is seen that artificial numerical oscillation associated with the point of singularity at the top left corner significantly reduces with the decrease in grid spacing and the plots have good match. The above results clearly establish that our newly developed integral vorticity condition is competent for high Re simulation.

4.4 Problem 4: Backward Facing Step Problem

Next we consider the flow over the backward-facing step in a channel. This problem is specifically chosen to test the applicability of the newly developed philosophy in open inflow and outflow situations. For this problem we employ compact discretization [15] in a multi-block structured grid. Sketch of the flow configuration along with the definition of length scales has been presented in Fig. 12. The backward-facing step has an expansion ratio $H/h = 2.0$, $h = 0.5$ over which the flow that develops in the upstream

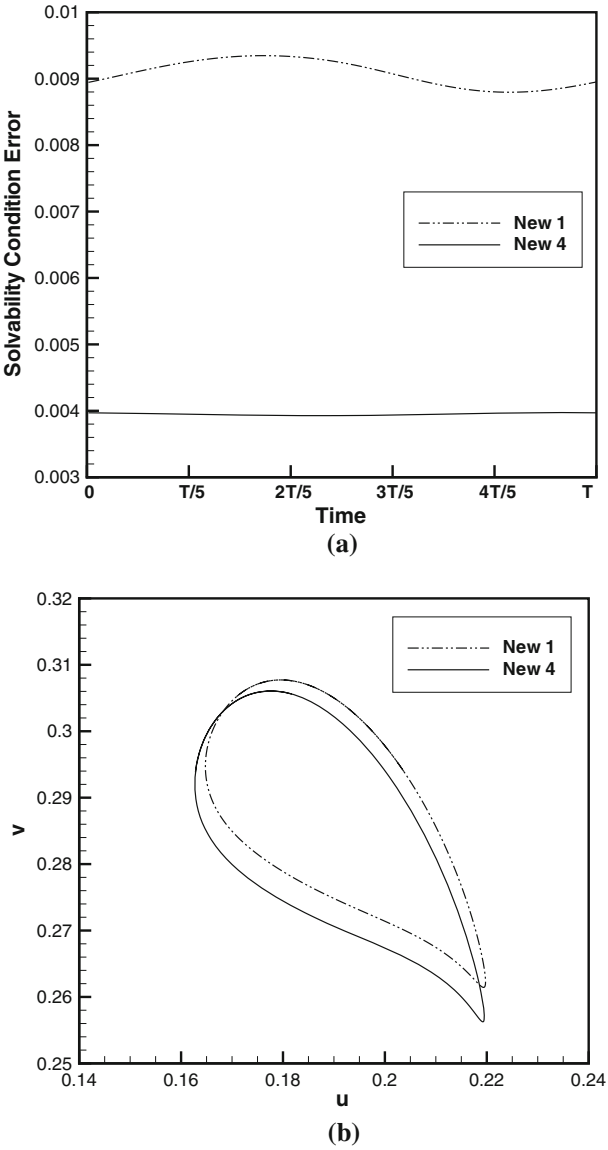

Fig. 9 Problem 3: **a** Extent to which solvability condition has been satisfied for $Re = 10{,}000$, **b** phase portrait of u versus v at the point $(2/16, 13/16)$ $Re = 10{,}000$

suddenly expands into a downstream channel. For this flow problem the Reynolds number is defined as $Re = \frac{2hU_{\text{avg}}}{\nu}$, U_{avg} being the average velocity at the inlet. At the inlet a parabolic velocity profile $u = 12y(1-2y)$, $v = 0$ has been prescribed and at the outlet convective boundary condition, given by $\frac{\partial \phi}{\partial t} + U_{\text{avg}} \frac{\partial \phi}{\partial x} = 0$, with ϕ standing for ψ, ψ_x and ψ_y, has been applied. For vorticity we use the boundary condition given by Eq. (8) at all the boundaries. This approach used for vorticity is new *vis-a-vis* approach adopted elsewhere [29,30]. An uniform grid with $\Delta x = 0.04$ and $\Delta y = 0.02$ has been used. We

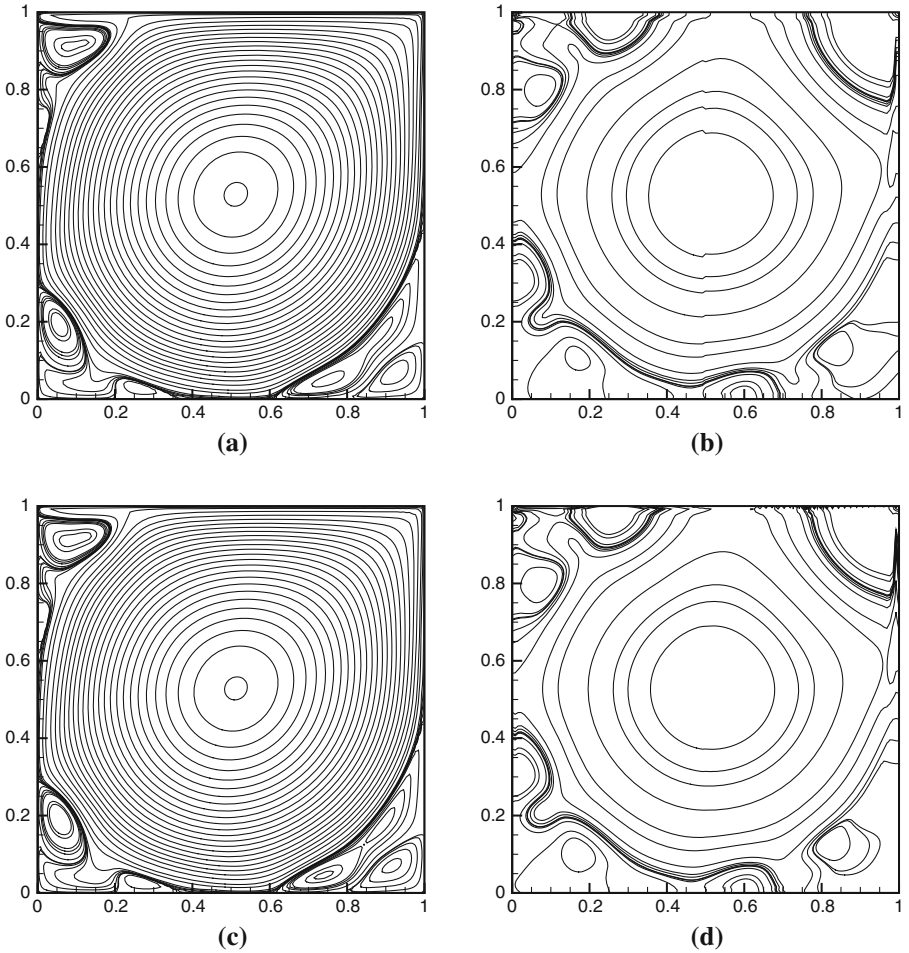

Fig. 10 Problem 3: Contours at periodic state for $Re = 10{,}000$ **a** streamfunction computed using New 1, **b** total pressure computed using New 1, **c** streamfunction computed using New 4, **d** total pressure computed using New 4

compute solutions to arrive at steady state for $Re = 100$ and 800 by taking $L_u = 6h$ and $L_d = 34h$. The streamfunction, vorticity and static pressure field have been shown in Fig. 13. A quantitative comparison of our results, obtained using the fourth order compact scheme developed by Sen [15], with that of Chiang and Sheu [29] has been done in Table 7. This comparison indicates validity of our newly developed boundary condition for vorticity.

4.5 Problem 5: Flow over a Circular Cylinder

Finally we consider flow past an impulsively started circular cylinder to verify the applicability of the newly developed boundary condition in open flow problems. The schematic diagram of the flow is shown in Fig. 14. We consider $R_\infty \approx 21$ and use a conformal transformation $x = \frac{1}{2}e^{\pi\xi}\cos\pi\eta$, $y = \frac{1}{2}e^{\pi\xi}\sin\pi\eta$ to transform the physical domain into a rectangular

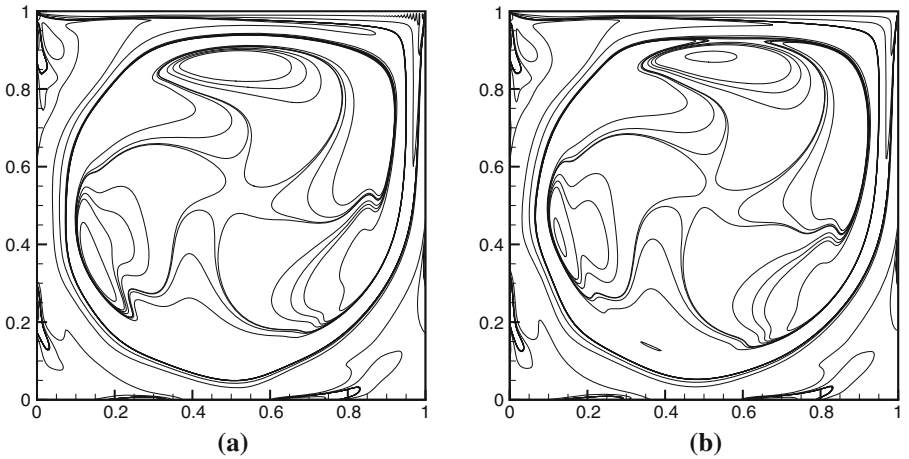

Fig. 11 Problem 3: Resolution check for vorticity contours at $Re = 10{,}000$ computed using New 1 with grid **a** 257×257, **b** 513×513

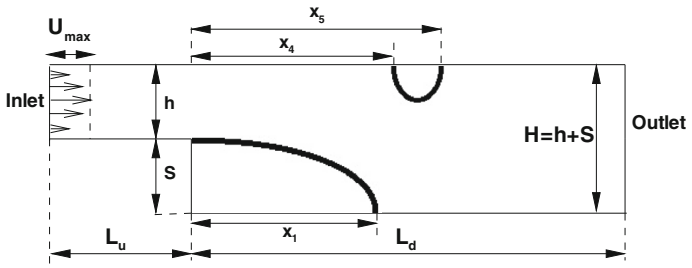

Fig. 12 Problem 4: Schematic diagram of the flow configuration and the definition of length scales

computational domain. Under such a transformation the streamfunction–vorticity formulation in Eqs. (1)–(2) is invariant up to a scaling factor, which enables the use of the scheme developed by Sen [15] in Cartesian grid. For streamfunction we use potential boundary condition in the upstream and convective boundary condition, appropriately translated onto the ξ–η plane, along the downstream far field. On the surface of the cylinder we set $\psi = 0$. For vorticity we use the newly developed boundary condition given by Eq. (8) at both the solid surface and the far field. No distinction has been made between the vorticity boundary conditions at upstream and downstream. To the best of our knowledge this is probably for the first time that identical vorticity boundary condition has been applied on all boundaries to simulate flow past an impulsively started circular cylinder. The Reynolds number for the flow is based on the diameter and we simulate flow for $Re = 100$ and 1000 using grids 121×201 and 169×281, respectively. For $Re = 100$ we use $\delta t = 0.01$ whereas for $Re = 1000$, $\delta t = 0.002$ has been considered for accurate simulation. A qualitative comparison of Strouhal numbers, drag and lift coefficients of the periodic state of flow for both the Reynolds numbers with the benchmark results available in the literature has been carried out in Table 8. A good quantitative comparison can be seen. To get an insight into the flow evolution under the new vorticity boundary condition we depict the time advancement of the drag and lift coefficients in Fig. 15. We present the streamlines and vorticity contours

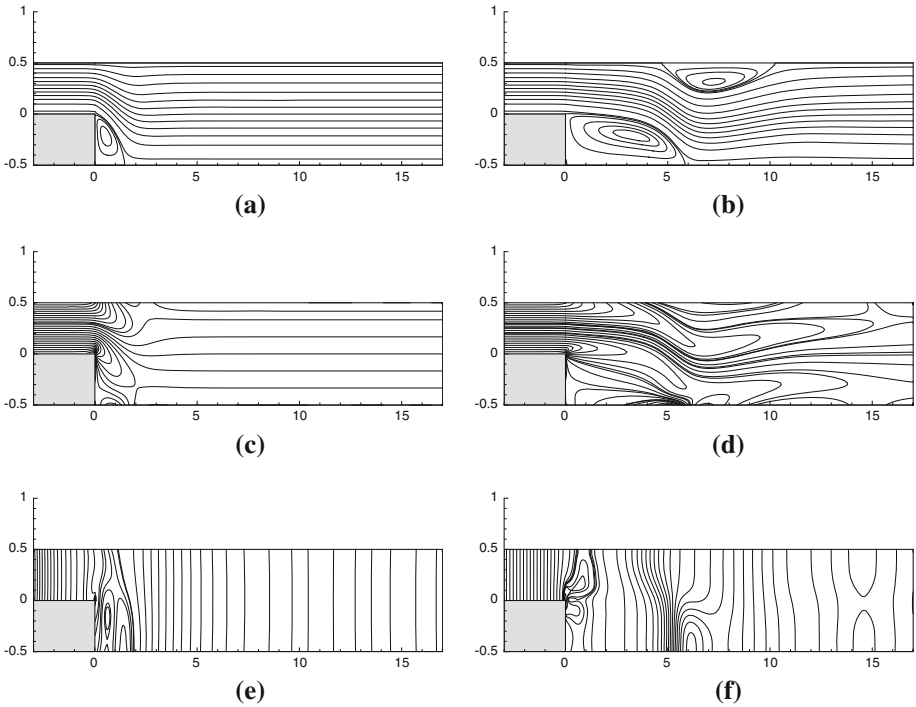

Fig. 13 Problem 4: Results for $Re = 100$ (*left*) and 800 (*right*). **a**, **b** Streamfunction. **c**, **d** Vorticity. **e**, **f** Static pressure

Table 7 Problem 4: Properties of the wall eddy for $Re = 100$ and 800

Wall	Re	100	800
Lower	Eddy centre (x, y)	(0.52, −0.22)	(3.2, −0.2)
	ψ_{value}	−0.0273	−0.0338
	Recirculation length x_1	1.48	5.88
		1.63 [29]	6.08 [29]
Upper	Eddy Centre (x, y)	–	(7.28, 0.32)
		–	
	ψ_{value}	–	0.5067
		–	
	Separation point x_4	–	4.72
		–	4.75 [29]
	Reattachment point x_5	–	10.28
		–	10.52 [29]

for the flows once the periodic state has been reached in Fig. 16. It can be seen that the new vorticity boundary condition is quite effective in creating vortices in the vicinity of the cylinder and is also able to convect the vortices out of the computational field at the far field boundary.

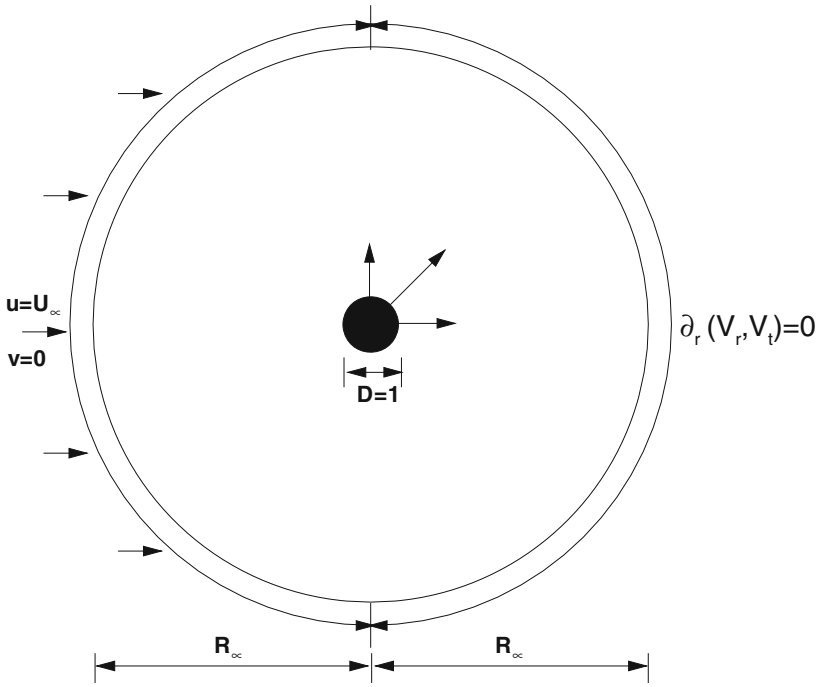

Fig. 14 Problem 5: Schematic diagram of the flow configuration

Table 8 Problem 5: Comparison of Strouhal numbers, drag and lift coefficients of the periodic flow

Re	Reference	*St*	C_D	C_L
100	Le et al. [31]	0.160	1.37 ± 0.009	± 0.323
	Berthelsen and			
	Faltinsen et al. [32]	0.169	1.38 ± 0.010	± 0.340
	Wang et al. [33]	0.170	1.379	± 0.357
	Present study	0.165	1.398 ± 0.007	± 0.207
1000	Chou and Huang [34]	0.22	1.39 ± 0.18	± 0.922
	Cheng et al. [35]	0.206	1.22 ± 0.15	± 1.1
	Qian and Vezza [36]	0.240	1.52 ± 0.22	± 1.41
	Present study	0.236	1.506 ± 0.172	± 0.986

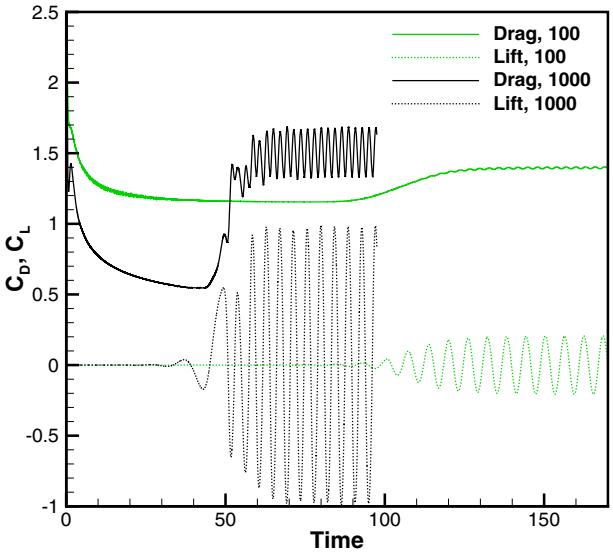

Fig. 15 Problem 5: Time evolution of the drag and lift coefficients for $Re = 100$ and 1000

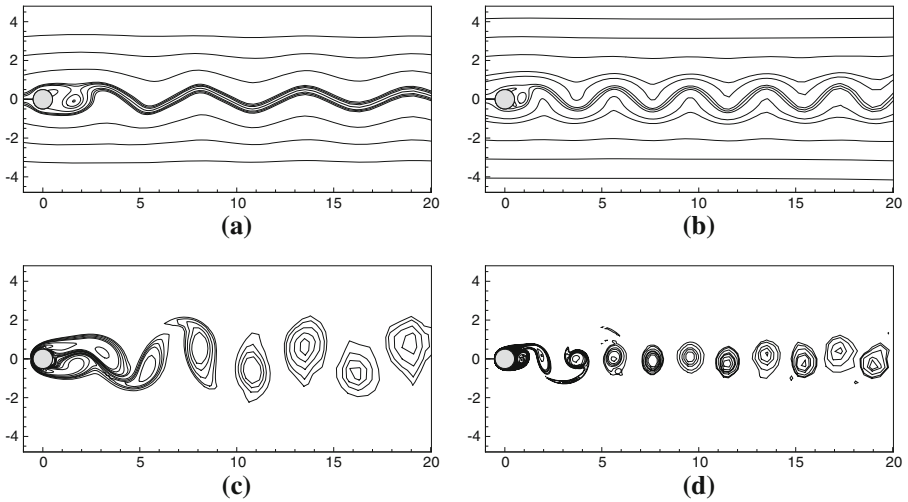

Fig. 16 Problem 5: Results for $Re = 100$ (*left*) and 1000 (*right*). **a**, **b** Streamfunction. **c**, **d** Vorticity

5 Conclusion

In this work we have designed an algorithm to implement a newly developed vorticity integral condition which can be used to compute solution of nonprimitive Navier–Stokes system. In this process we have established a modified vorticity boundary condition. This new condition can be realized using an explicit formula. It can tackle both the wall bounded and open flow problems with ease. Various different implementations of this integral condition in juxtaposition to the finite volume approach have been outlined. Stability and convergence analysis of the boundary discretization procedures are also carried out. These approaches have

been compared with as many as six existing local boundary conditions. We have also shown that this new integral condition has linkages with some of the existing vorticity boundary conditions. A model problem that embodies the essential features of the incompressibility and viscosity has been used to reveal important characteristics of the new formulation. For all the three different benchmark problems, discussed in this work, the newly developed algorithm has been found to be quite suitable. It is worthwhile to note that probably for the first time identical conditions for computing vorticity have been used on all boundaries for flow past impulsively started circular cylinder. The newly developed algorithm permits smooth and precise convalescence of vorticity. In addition we have also obtained correct pressure field for both the attached and separated boundary layer flows.

Acknowledgements The first author is thankful to Dr. Deepjyoti Goswami, Department of Mathematical Sciences, Tezpur University, India for some intense discussions. Both the authors are grateful to the anonymous reviewers for their comments and suggestions.

References

1. Gatski, T.B.: Review of incompressible fluid flow computations using the vorticity–velocity formulation. Appl. Numer. Math. **7**, 227–239 (1991)
2. Gupta, M.M., Kalita, J.C.: A new paradigm for solving Navier–Stokes equations: streamfunction-velocity formulation. J. Computat. Phys. **207**, 52–68 (2005)
3. Roache, P.J.: Computational Fluid Dynamics. Hermosa Publishers, New Mexico (1976)
4. Weinan, E., Liu, J.-G.: Vorticity boundary condition and related issues for finite difference schemes. J. Comput. Phys. **124**, 368–382 (1996)
5. Napolitano, M., Pascazio, G., Quartapelle, L.: A review of vorticity conditions in the numerical solution of the $\zeta - \psi$ equations. Comput. Fluids **28**, 139–185 (1999)
6. Thom, A.: The flow past circular cylinders at low speeds. Proc. R. Soc. Lond. **141**, 651–669 (1933)
7. Huang, H., Wetton, B.R.: Discrete compatibility in finite difference methods for viscous incompressible fluid flow. J. Comput. Phys. **126**, 468–478 (1996)
8. Orszag, S.A., Israeli, M.: Numerical simulation of viscous incompressible flows. Annu. Rev. Fluid Mech. **6**, 281–318 (1974)
9. Olson, M.D., Tuann, S.Y.: New finite element results for the square cavity. Comput. Fluids **7**, 123–135 (1979)
10. Schreiber, R., Keller, H.B.: Driven cavity flows by efficient numerical techniques. J. Comput. Phys. **49**, 310–333 (1983)
11. Sen, S., Kalita, J.C., Gupta, M.M.: A robust implicit compact scheme for two-dimensional unsteady flows with a biharmonic streamfunction formulation. Comput. Fluids **84**, 141–163 (2013)
12. Quartapelle, L., Valz-Gris, F.: Projection conditions on the vorticity in viscous incompressible flows. Int. J. Numer. Methods Fluids **1**, 129–144 (1981)
13. Chorin, A.J.: Vortex sheet approximation of boundary layers. J. Comput. Phys. **27**, 428–442 (1978)
14. Anderson, C.R.: Vorticity boundary conditions and boundary vorticity generation for two-dimensional viscous incompressible flows. J. Comput. Phys. **80**, 72–97 (1989)
15. Sen, S.: A new family of (5,5) CC-4OC schemes applicable for unsteady Navier–Stokes equations. J. Comput. Phys. **251**, 251–271 (2013)
16. Chung, T.J.: Computational Fluid Dynamics. Cambridge University Press, Cambridge (2002)
17. Kelly, C.T.: Iterative Methods for Linear and Nonlinear Equations. SIAM Publications, Philadelphia (1995)
18. Abdallah, S.: Numerical solutions for the pressure Poisson equation with Neumann boundary conditions using a non-staggered grid. J. Comput. Phys. **70**, 182–192 (1987)
19. Wang, C., Liu, J.-G.: Analysis of finite difference schemes for unsteady Navier–Stokes equations in vorticity formulation. Numer. Math. **91**, 543–576 (2002)
20. Wang, C.: A general stability condition for multi-stage vorticity boundary conditions in incompressible fluids. Methods Appl. Anal. **15**, 469–476 (2008)
21. Peyret, R., Taylor, T.: Computational Methods for Fluid Flow. Springer, New York (1983)
22. Briley, W.R.: A numerical study of laminar separation bubbles using Navier–Stokes equations. J. Fluid Mech. **47**, 713–736 (1971)

23. Woods, L.C.: A note on the numerical solution of fourth-order differential equations. Aeronaut. Q **5**, 176–182 (1954)
24. D'Alessio, S.J.D., Dennis, S.C.R.: A vorticity model for viscous flow past a cylinder. Comput. Fluids **23**, 279–293 (1994)
25. Sanyasiraju, Y.V.S.S., Manjula, V.: Flow past an impulsively started circular cylinder using a higher-order semicompact scheme. Phys. Rev. E **72**, 0167091–01670910 (2005)
26. Dipankar, A., Sengupta, T.K., Talla, S.B.: Suppression of vortex shedding behind a circular cylinder by another control cylinder at low Reynolds numbers. J. Fluid Mech. **573**, 171–190 (2007)
27. Orszag, S.A., Israeli, M., Deville, M.O.: Boundary conditions for incompressible flows. J. Sci. Comput. **1**, 75–111 (1986)
28. Ghia, U., Ghia, K.N., Shin, C.T.: High-Re solutions for incompressible flow using the Navier–Stokes equations and a multigrid method. J. Comput. Phys. **48**, 387–411 (1982)
29. Chiang, T.P., Sheu, T.W.H.: A numerical revisit of backward-facing step flow problem. Phys. Fluids **11**, 862–874 (1999)
30. Biswas, G., Breuer, M., Durst, F.: Backward-facing step flows for various expansion ratios at low and moderate Reynolds numbers. Trans. ASME **126**, 362–374 (2004)
31. Le, D.V., Khoo, B.C., Peraire, J.: An immersed interface method for viscous incompressible flows involving rigid and flexible boundaries. J. Comput. Phys. **220**, 109–138 (2006)
32. Berthelsen, P.A., Faltinsen, O.M.: A local directional ghost cell approach for incompressible viscous flow problems with irregular boundaries. J. Comput. Phys. **227**, 4354–4397 (2008)
33. Wang, Z., Fan, J., Cen, K.: Immersed boundary method for the simulation of 2D viscous flow based on vorticity–velocity formulations. J. Comput. Phys. **228**, 1504–1520 (2009)
34. Chou, M.-H., Huang, W.: Numerical study of high-Reynolds-number flow past a bluff object. Int. J. Numer. Methods Fluids **23**, 711–732 (1996)
35. Cheng, M., Chew, Y.T., Luo, S.C.: A hybrid vortex method for flows over a bluff body. Int. J. Numer. Methods Fluids **24**, 253–274 (1997)
36. Qian, L., Vezza, M.: A vorticity-based method for incompressible unsteady viscous flows. J. Comput. Phys. **172**, 515–542 (2001)